DYNAMICAL CORRELATIONS OF MULTIPLY SCATTERED LIGHT

D. J. PINE[ab], D. A. WEITZ[a], G. MARET[c], P. E. WOLF[d], E. HERBOLZHEIMER[a], and P. M. CHAIKIN[ae]

[a] *Exxon Research and Engineering*
Route 22 East, Annandale
New Jersey 08801, USA

[b] *Department of Physics*
Haverford College, Haverford
Pennsylvania 19041, USA

[c] *Hochfeld Magnetlabor*
Max Planck Institut für Festkörperforschung 166x
F-38042 Grenoble-Cedex, France

[d] *Centre de Recherches sur les Très Basses Températures, CNRS*
F-38042 Grenoble-Cedex, France

[e] *Department of Physics*
Princeton University, Princeton
New Jersey 07895, USA

Motion of particles in optically dense media gives rise to temporal fluctuations in the intensity of multiply scattered light. We show that useful information about the dynamics of the scatterers can be obtained

from measurements of the temporal autocorrelation functions of these fluctuations in the multiply scattered light. We develop a phenomenological theory, which models the transport of light as a random walk between scatterers, and obtain explicit expressions for the autocorrelation functions for several experimental geometries. These expressions are compared with experiments probing the dynamics of colloidal suspensions and are shown to be in excellent agreement with the data. The dependence of the autocorrelation functions on the experimental geometry provides a powerful means of exploring the particle dynamics over vastly different length and time scales. Thus, this technique extends the conventional single scattering technique of Dynamic Light Scattering to the multiple scattering regime. We call this new technique Diffusing Wave Spectroscopy (DWS). We illustrate the power of DWS by applying it to measure the particle size in concentrated suspensions and to study the diffusion of particles in porous media and the flow of particles under shear. In addition, we show that DWS can be extended to study the dynamics of interacting colloids by including the consequences of the correlations between the particle positions and velocities. DWS can also be used to study the nature of the transport of light in disordered systems and, in particular, the limitations of using a continuum diffusion approximation. To exploit this, we show that other quantities, such as the angular dependence of the coherent backscattering cone and the absorption dependence of the incoherent backscattering intensity, depend on the distribution of light paths through the sample in the same way as the temporal autocorrelation functions obtained in backscattering.

Contents

1. INTRODUCTION

A characteristic feature of the scattering of light from any random medium is the existence of a very strong spatial modulation of the scattered intensity called the speckle pattern. The speckles are due to the addition of the electric fields, with random phases, scattered from different illuminated points. This feature is characteristic not only of light, but also of any scattering phenomenon that can be described in terms of waves. It also results from multiply scattered light just as it does from singly scattered light. If the scattering medium is perfectly stationary, the speckle pattern will also be stationary. By contrast, if the positions of the scatterers in the medium change with time, the speckle pattern will also evolve with time. Therefore, the intensity of the scattered light at any point will fluctuate. Typically, the motion of the scatterers will occur on a time scale that is much longer than any propagation time of the light through the medium. Thus, the fluctuations in the scattered light intensity will reflect the dynamics of the scatterers.

In this chapter, we discuss the analysis of these temporal fluctuations of the intensity for the case of multiply scattered light, and determine the temporal autocorrelation function of the scattered intensity. We present a heuristic approach to derive the functional form of this autocorrelation function. This approach exploits the diffusion approximation to describe the transport of light in the strongly multiple scattering regime. The expressions derived are compared with experiment for several important geometries and are shown to be in remarkably good agreement. Furthermore, we show that useful information about the dynamics of the scattering medium can be recovered from our expressions for the autocorrelation functions.

The analysis of the temporal fluctuations of the scattered intensity in the strictly single scattering regime is a well developed and extremely powerful spectroscopy which is variously called quasielastic light scattering (QELS), dynamic light scattering, or photon correlation

spectroscopy.[1,2] In this technique, knowledge of the scattering vector, q, is crucial as it sets the length scale over which particle motion is probed. Extensions of QELS to the multiple scattering regime have proved extremely difficult and have been limited essentially to only doubly scattered light.[3] In turn, this has severely limited the application of QELS to the singly scattering regime. By contrast, in the very strong multiple scattering regime, it is possible to exploit the diffusive nature of the transport of light and again obtain useful information about the particle dynamics.[4,5,6] We call this new technique diffusing wave spectroscopy (DWS).[7,8] In this chapter, we demonstrate the potential of DWS both in extending QELS to the multiple scattering regime and in studying the particle dynamics of interacting systems.

The analysis of the temporal intensity fluctuations also provides a unique probe of the nature of transport of light in strongly scattering media, complementing the many studies of the static properties of multiply scattered light (see the review by Lagendijk *et al.* in this volume).[9,10] To make this explicit, we show that there exists a direct analogy between the time dependence of the temporal autocorrelation function of the backscattered intensity and the angular dependence of the coherent enhancement of the static backscattered intensity.[11] Physically this arises from the fact that both measurements probe the same type of sum over light diffusion paths. In the case of the enhanced backscattering, these paths contribute to the increase of the scattered intensity, while in the case of the dynamics, they contribute to the decay of the autocorrelation function. We can, therefore, use the autocorrelation function as a sensitive experimental measure of the light diffusion paths. In particular, it provides a means of probing the limitations of the continuum nature of the diffusion approximation in describing the contributions of the very short scattering paths.

The temporal autocorrelation function of the intensity in one or more speckles is the most convenient quantitative measure of the dynamics of the scattered light. In the single scattering regime, the characteristic time dependence of the fluctuations is determined by the

particle motion over the length scale set by q^{-1}, where the wavevector is $q = (4\pi n/\lambda)\sin(\theta/2)$, with λ the wavelength, n the index of refraction of the medium, and θ the scattering angle. Thus, particle motion is probed over length scales of λ and larger. By contrast, in the multiple scattering regime, the characteristic time dependence is determined by the cumulative effect of many scattering events and, thus, the characteristic time scales are much faster. Consequently, particle motion is probed over length scales much smaller than λ.

This is illustrated in Fig. 1, where we show intensity autocorrelation functions from suspensions of 0.497-μm diameter spheres at vastly different concentrations. The data for Fig. 1(a) are obtained at a scattering angle of $\theta = 90°$ from an essentially transparent suspension of volume fraction $\phi = 10^{-5}$, which is in the single scattering regime. It is a single exponential, reflecting only one characteristic time scale $(Dq^2)^{-1}$, where D is the particle diffusion coefficient. By contrast, the data in Fig. 1(b) are obtained in a backscattering geometry from a suspension with $\phi = 0.01$ which is in the strongly multiple scattering regime, and therefore appears white. It is both highly non-exponential and has a substantially faster initial decay than the single scattering data. However, the volume fraction of the suspension is still sufficiently low that the diffusion coefficient of the particles is unchanged from the dilute limit. Thus, the more rapid initial decay and non-exponential shape must arise from the much larger number of scattering events. The data for Fig. 1(c) are obtained for the same concentration, $\phi = 0.01$, but from light transmitted through a sample of thickness, $L = 2$mm. Its decay is even more rapid, although more nearly exponential. This reflects a larger average number of scattering events due to the more important contributions of longer paths to the transmitted light as compared to the backscattered light.

This chapter is organized as follows: In the next section, we discuss the extension of the traditional approach for QELS to the multiple scattering regime. We calculate the intensity autocorrelation function within the diffusion approximation for the transport of light and then

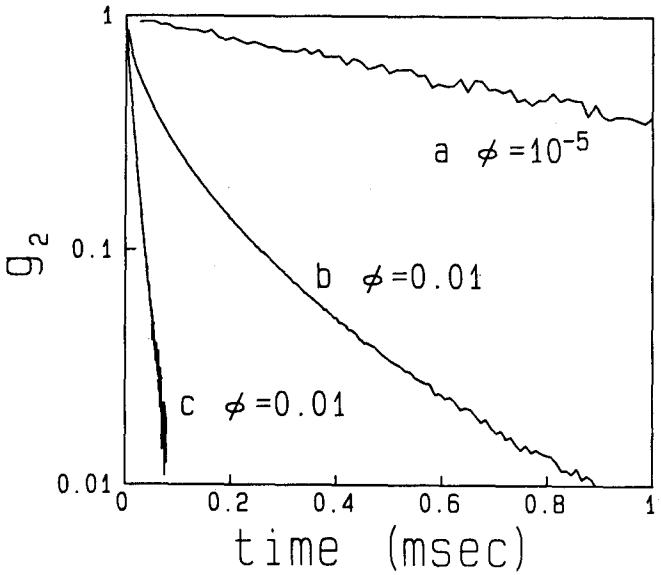

Fig. 1. Temporal intensity autocorrelation functions from aqueous suspensions of 0.497-μm-diameter polystyrene spheres at different volume fractions, ϕ, and for different scattering geometries: (a) single scattering, $\phi = 10^{-5}$, $\theta = 90°$; (b) multiple scattering, $\phi = 0.01$, backscattering from a thick sample; (c) multiple scattering, $\phi = 0.01$, transmission through a 2-mm-thick sample.

obtain explicit functional forms of the complete intensity autocorrelation function for several important experimental geometries. The predictions are compared to the experimental results for transmission and backscattering geometries. In the next section, we demonstrate how DWS can provide a sensitive new probe of the nature of the transport of light in the multiple scattering regime by comparing the short-time behavior of the temporal autocorrelation functions to the angular dependence of the static coherent backscattering and the absorption dependence of the incoherent backscattered intensity. Finally, we illustrate the utility of DWS for studying the dynamics of particles in the multiple scattering regime.

2. THEORY

Two theoretical approaches have been used to calculate the temporal autocorrelation function of multiply scattered light. One approach is to start from the wave equation for the propagation of light and to use a diagrammatic description of the scattering from the random fluctuations in the dielectric constant. The consequences of motion of the scatterers was first considered by Golubentsev[1,2] and the actual temporal correlation functions were calculated by Stephen.[6] By constrast, the second approach considers the diffusive transport of individual photons directly, rather than starting from the wave equation.[4,5,7,8] The path of each photon is determined by random, multiple scattering from a sequence of particles. The loss of correlations due to the motion of scatterers is calculated for each light path. The contributions of all paths, appropriately weighted, are then summed to obtain the temporal autocorrelation function.

In this chapter, we adopt the second approach. It is mathematically simpler and physically more transparent than the diagrammatic methods. It can also be more readily generalized to larger particles which scatter light anisotropically and are typical of media which exhibit multiple scattering of light. The key to this approach is to model the transport of each photon through the sample as a random walk. This is done within the diffusion approximation, which allows the weighting of each path to be determined, and simplifies the calculation of the temporal autocorrelation.

We begin by considering a single light path and calculate its contribution to the decay of the autocorrelation function. For simplicity we consider independent spherical scatterers of uniform size undergoing Brownian motion. The fluctuating phase of the multiply scattered light caused by the motion of all the particles in the path leads to the decay of the autocorrelation function which, for a path of n scattering events, is given by

$$G_1^{(n)}(\tau) \equiv \langle E^{(n)*}(0)E^{(n)}(\tau)\rangle = \langle |E^{(n)}(0)|^2\rangle e^{-i\Delta\phi^{(n)}}(\tau) \; . \qquad (1)$$

Here $E^{(n)}$ is the contribution to the scattered electric field from a path of order n and $\Delta\phi^{(n)}(\tau)$ is the *total* change in its phase due to the motion of all n scatterers,

$$\Delta\phi^{(n)}(\tau) = \sum_{i=1}^{n} \mathbf{q}_i \cdot \Delta\mathbf{r}_i(\tau) \ , \tag{2}$$

where $\mathbf{q}_i$ is the scattering wavevector (proportional to the momentum transfer) of the ith scattering event and $\Delta\mathbf{r}_i(\tau) = \mathbf{r}_i(\tau) - \mathbf{r}_i(0)$ is the change in position of the ith scattering particle in a time τ. Assuming that the fields belonging to different paths add incoherently, the average contribution of all paths of order n to the autocorrelation function becomes

$$G_1^{(n)}(\tau) = I_0 P(n) \left\langle \prod_{i=1}^{n} e^{-i\mathbf{q}_i \cdot \Delta\mathbf{r}_i(\tau)} \right\rangle \tag{3}$$

where $P(n)$ is the fraction of the total scattered intensity I_0 in the nth order paths. The total field autocorrelation function $G_1(\tau)$ is obtained by summing over n,

$$G_1(\tau) = I_0 \sum_{n=1}^{\infty} P(n) \left\langle \prod_{i=1}^{n} e^{-i\mathbf{q}_i \cdot \Delta\mathbf{r}_i(\tau)} \right\rangle \ . \tag{4}$$

This sum can be evaluated directly by computer simulation.[13] While this approach can yield accurate results, it is useful to have analytic expressions for $G_1(\tau)$. To this end, we assume that the dominant contribution to Eq. (4) comes from light paths with many scattering events, that is, large n. For large n, the transport of light through a sample can be accurately described within the diffusion approximation. This, in turn, allows $P(n)$ and the averages in Eq. (4) to be easily evaluated.

For large n, we can relax the condition that the sum of the intermediate scattering vectors must equal the difference between the incident and exiting wavevectors, $\Sigma_i \mathbf{q}_i = \mathbf{k}_n - \mathbf{k}_0$, and assume that successive scattering events are uncorrelated. This corresponds to a random distribution of the q_i. Then, for independent particles, the

right hand side of Eq. (3) becomes $P(n)\langle\exp[-i\mathbf{q}\cdot\Delta\mathbf{r}(\tau)]\rangle^n$ where $\langle\rangle$ denotes averages over both the particle motion $\Delta\mathbf{r}(\tau)$ and the distribution of wavevectors $\mathbf{q}$. For Brownian motion, the distribution of $\Delta\mathbf{r}(\tau)$ is Gaussian and the average over particle motion is readily performed yielding

$$G_1^{(n)}(\tau) = I_0 P(n)\,\langle e^{-q_i^2\langle\Delta r^2(\tau)\rangle/6}\rangle_q^n \ , \tag{5}$$

where $\langle\Delta r^2(\tau)\rangle = 6D\tau$ and now $\langle\,\rangle_q$ denotes the average over q. Thus, Eq. (5) implies that the relaxation rate will be large for paths with large n, independent of the average over q.

The average over q can be performed explicitly for point-like scatterers, which scatter light isotropically; this gives[6,12]

$$G_1^{(n)}(\tau) = I_0 P(n)\left[\frac{\tau_0}{4\tau}\left(1 - e^{-4\tau/\tau_0}\right)\right]^n \ , \tag{6}$$

where $\tau_0 \equiv (Dk_0^2)^{-1}$. However, for larger particles which scatter light anisotropically, the average over $\mathbf{q}$ is more difficult to perform. Thus, we restrict ourselves to small delay times $\tau \ll \tau_0$ and retain only the first term in a cumulant expansion,[4]

$$\left\langle e^{-Dq^2\tau}\right\rangle_q^n \simeq \langle 1 - Dq^2\tau\rangle_q^n = (1 - D\langle q^2\rangle\tau)^n \simeq e^{-D\langle q^2\rangle\tau n} \ . \tag{7}$$

We can compare this more general approximation with the exact expression, Eq. (6), for point-like scatterers by evaluating $\langle q^2\rangle$ for a flat distribution

$$\langle q^2\rangle = \int q^3\,dq \Big/ \int q\,dq = 2k_0^2$$

which gives

$$G_1^{(n)}(\tau) = I_0 P(n) e^{-(2\tau/\tau_0)n} \ . \tag{8}$$

Expanding the exact expression in Eq. 6 gives

$$G_1^{(n)}(\tau) = I_0 P(n) e^{-2n\tau/\tau_0[1-1/3(\tau/\tau_0)+O(\tau/\tau_0)^3]}$$

so that the cumulant expansion gives the correct results to leading order in τ/τ_0. Furthermore, the effective decay time is $\tau_0/2n$, so for large

$n, G_1^{(n)}(\tau)$ decays essentially to zero before the higher order terms make a significant contribution. Nevertheless, for large τ/τ_0 the cumulant expansion fails since the exact expression in Eq. (6) decays as a power law, $(\tau/\tau_0)^{-n}$, due to the contribution of scattering with small q. However, at these long times low order scattering events dominate. For small n, the distribution of $\mathbf{q}_i$ is not random but must satisfy the condition that $\Sigma_i \mathbf{q}_i = \mathbf{k}_n - \mathbf{k}_0$. This will modify the average in Eq. (6) and could have the effect of at least partially offsetting the error introduced by the cumulant expansion.[14]

The approximate expression can be easily generalized to treat the anisotropic scatterers typically used in experiments. Here, the single particle scattering intensity is peaked in the forward direction and $\langle q^2 \rangle$ is less than $2k_0^2$. Physically, this means that more scattering events will be required to randomize the direction of light propagation. The length scale over which this randomization occurs is the transport mean free path, l^* (Refs. 15,16). For anisotropic scatterers, l^* is generally greater than the scattering mean free path, l, the mean distance between scattering events. It is the transport mean free path which is related to the diffusion coefficient for multiply scattered light, $D_l = cl^*/3$, where c is the speed of light in the medium.

We estimate l^* by analogy to the calculation of the effective length of a statistical segment in semiflexible polymers.[17] Thus, we sum the projections of all steps of length l in a long path onto the direction of the first step. Then

$$l^* = l \sum_{i=1}^{n} \langle \cos\theta \rangle^i$$

where $\langle \cos\theta \rangle$ is the average angle between successive steps. For large n, this becomes

$$l^* = l/(1 - \langle \cos\theta \rangle) \ .$$

Since $\langle 1 - \cos\theta \rangle = \langle 2\sin^2(\theta/2) \rangle = 2\langle q^2 \rangle/(2k_0)^2$, we find

$$2\langle q^2 \rangle/(2k_0)^2 = l/l^* \ .$$

Therefore *both* $\langle q^2 \rangle$ and l^* are simply obtained by averaging over the angular dependence of the form factor $F(\mathbf{q})$ of the scatterers

$$\langle q^2 \rangle = 2k_0^2 \frac{l}{l^*} = \int q^2 F(\mathbf{q})\, d\mathbf{q} \Big/ \int F(\mathbf{q})\, d\mathbf{q} \,. \tag{9}$$

It follows from Eqs. (5), (7), and (9) that for anisotropic scatterers, the contribution of an nth order scattering path is

$$G_1^{(n)}(\tau) = I_o P(n) e^{-(2\tau/\tau_0)(l/l^*)n} \,. \tag{10}$$

We note that the accuracy of Eq. (10) improves as the scattering becomes more anisotropic. The second cumulant of $\langle e^{-Dq^2\tau} \rangle$ is $e^{-\frac{1}{2}(D\tau)^2[\langle q^4 \rangle - \langle q^2 \rangle^2]}$. For typical form factors, $F(q)$, we expect $\langle q^4 \rangle$ to scale as $\langle q^2 \rangle^2$ so that the cumulant expansion in Eq. (7) should be valid to leading order in $D\langle q^2 \rangle \tau \simeq (\tau/\tau_0)(l/l^*)$. Thus, for large scatterers, where $l^* \gg l$, the range of validity of Eq. (10) may extend up to $\tau \simeq \tau_0$.

The total field autocorrelation function $G_1(\tau)$ is obtained by summing over scattering paths of all orders

$$G_1(\tau) = I_0 \sum_{n=1}^{\infty} P(n) e^{-(2\tau/\tau_0)(l/l^*)n} \,.$$

If we rescale n by defining $n^* = (l/l^*)n$, the exponential term in this equation is identical to Eq. (8) for isotropic scatterers. Furthermore, in the diffusion approximation, $P(n)$, the fraction of photons which travel a path of length $s = nl$ through the scattering medium, is a function of n^* rather than n, because the characteristic length scale of the light propagation is the transport mean free path, l^*, rather than the scattering mean free path, l. As a result, in this approximation,

$$G_1(\tau) = I_0 \sum_{n^*=1}^{\infty} P(n^*) e^{-(2\tau/\tau_0)n^*} \,. \tag{11}$$

This reflects a renormalization of the mean free path for anisotropic scatterers, so that the light may be viewed as undergoing an isotropic

random walk with an average step length l^*. Finally, we note that the decay rate of a given path depends critically on its length. Long paths reflect the aggregate contribution of many scattering events. Thus, each particle need move only a small distance for the total path length to change by a wavelength. This occurs in a short time, leading to a rapid decay rate. By contrast, short paths reflect the contribution of a small number of scattering events. Thus, each particle must undergo substantial motion for the total path length to change by a wavelength. This takes a longer time, leading to a slower decay.

The key to the solution of Eq. (11) is the determination of $P(n^*)$. This task is greatly simplified if we restrict ourselves to the continuum limit. Thus, we approximate the summation over n^* by an integral over the path lengths, $s = n^* l^*$, and obtain

$$G_1(\tau) = \langle E(0)E^*(\tau)\rangle = I_o \int P(s) e^{-(2\tau/\tau_0)s/l^*} ds \ . \qquad (12)$$

In this case, $P(s)$ is the fraction of photons which travel a path of length s through the scattering medium. Now we can use the diffusion approximation to describe the random walk of the light, and $P(s)$ can be obtained from the solution of the diffusion equation for the appropriate experimental geometry. We emphasize, however, that the continuum approximation to the discrete scattering events will break down whenever there are significant contributions from short light paths.

Physically, we can regard $P(s)$ as giving the distribution of path lengths of the light diffusing through the sample. In general, $P(s)$ depends on geometrical factors such as the size and shape of the sample cell and incident light beam. As we shall see, $P(s)$ can be determined for many different scattering geometries of experimental interest. First, however, it is instructive to consider the results for a case where the physics and mathematics are simple, but the experiment is quite difficult.

We consider a scattering medium of infinite extent and introduce the diffusing light at a point inside the medium. The light is detected

at a point a distance r away. If r is much larger than l^*, then $P(s)$ is given by the usual Gaussian distribution which results from the central limit theorem,

$$P(s) = \left(\frac{3}{4\pi n^* l^{*2}}\right)^{3/2} e^{-3r^2/4n^* l^{*2}} = \left(\frac{3}{4\pi s l^*}\right)^{3/2} e^{-3r^2/4sl^*} , \quad (13)$$

where $n^* = s/l^*$ is the number of steps.[15] In Fig. 2 we show a plot of Eq. (13) as a function of path length s. As expected, $P(s)$ reaches a maximum when $s_{\max} \approx (r/l^*)^2 l^*/2$, which corresponds to a random walk with $n^* = (r/l^*)^2/2$ steps. For very short paths $P(s) \to 0$, since the light must diffuse a distance r before it can be detected at all. Thus the relative probability of having random walks with path lengths $s \ll s_{\max}$ is small. For long paths, $s \gg s_{\max}$, $P(s)$ decays very slowly according to a power law, $s^{-3/2}$.

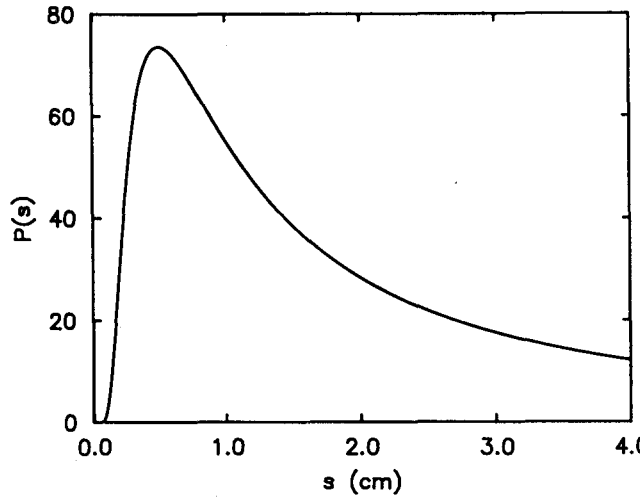

Fig. 2. $P(s)$ *vs* s: The fraction of photons which travel a distance s between a point source and a point detector separated by a distance r in an infinite random medium with strong multiple scattering. (Eq. (13), with $l^* = 100$ μm and $r = 1$ mm).

Using this simple form for the distribution of path lengths we can combine Eqs. (12) and (13) and obtain an expression for the temporal

autocorrelation function

$$G_1(\tau) = I_0 \int_0^\infty \left(\frac{3}{4\pi s l^*}\right)^{3/2} e^{-3r^2/4sl^* - (2\tau/\tau_0)s/l^*} ds \,. \qquad (14)$$

Some insight into the behavior of $G_1(\tau)$ as a function of delay time can be obtained using the method of steepest descents. Thus, the dominant contribution to the integral occurs when the argument of the exponential is at its maximum value,

$$\frac{\partial}{\partial s}\left(-\frac{3r^2}{4sl^*} - \frac{2\tau}{\tau_0}\frac{s}{l^*}\right) = \frac{3r^2}{4s^2 l^*} - \frac{2\tau}{\tau_0 l^*} = 0$$

giving

$$s_d = r\sqrt{\frac{3\tau_0}{8\tau}} \,.$$

Thus, the length, s_d, of the paths which dominate the correlation function decreases with increasing delay time. Performing the integral in Eq. (14), we obtain an explicit expression for the autocorrelation function,

$$G_1(\tau) \propto e^{-(r/l^*)\sqrt{6\tau/\tau_0}} \,.$$

Since for $\tau \to 0$, $\partial G_1/\partial\tau \to -\infty$, at the shortest delay times, the autocorrelation function decays very quickly. This reflects the divergence of s_d as $\tau \to 0$. The square root dependence arises from the form of the exponential cut-off of the short paths. However, the singularity at short times results from the fact that the contributions of $P(s)$ to the autocorrelation function are only a slowly decaying function of path length ($s^{-3/2}$). This singularity is a characteristic feature of any multiple scattering geometry which contains significant contributions from infinitely long paths, where $P(s) \sim s^{-3/2}$. As discussed below, this singularity is observed in backscattering from a semi-infinite sample, but not in transmission through a finite slab.

To describe experimental data, we must solve Eq. (12) to obtain the autocorrelation function for physically realizable geometries, where

the mathematics are more complex but the experiment is simpler. Restricting ourselves to the continuum approximation, $P(s)$ can be obtained from the solution of the diffusion equation for the appropriate geometry. In fact we can further simplify our task by extending the limits of the integration in Eq. (12) from $s = 0$ to $s = \infty$, which makes $G_1(\tau)$ a Laplace transform of $P(s)$. Then we can solve the Laplace transform of the diffusion equation to obtain the desired autocorrelation function directly. However, we again emphasize the limitations in this approach. Extending the lower bound of the integral to $s = 0$ may allow unphysically short paths to contribute to the autocorrelation function, depending on the scattering geometry. Furthermore, the short paths cannot be properly treated within the continuum approximation inherent in the diffusion equation. Thus, this approach is strictly valid only for long paths, where the diffusion approximation is a good description of the transport of light. Nevertheless, the great simplicity afforded by this approach makes it worthwhile to try to extend its applicability to more general geometries.

Physical insight into the method for determining $P(s)$ by solving the diffusion equation can be obtained by considering a simple experiment. An instantaneous pulse of light is incident on the face of a sample which multiply scatters the light. The scattered photons will execute a random walk until they either escape the sample or arrive at the point $\mathbf{r}_d$ on the boundary where the light is detected. The intensity of light that reaches $\mathbf{r}_d$ is zero at $t = 0$, then increases to a maximum, and finally decreases back to zero at long times when all the photons have left the sample. At time t, the photons arriving at point $\mathbf{r}_d$ are those that have traveled a path length $s = ct$ through the sample. Thus, the time dependence of the intensity of light arriving at point $\mathbf{r}_d$ is directly proportional to $P(s)$. The details of this time dependence, and hence the shape of $P(s)$, will depend on the experimental geometry.

To obtain $P(s)$ for a given experimental geometry, we must use the diffusion equation to determine the dispersion induced in a delta function pulse as it traverses the scattering medium. To accomplish

this, we denote the density of diffusing photons within the medium by $U(\mathbf{r})$. Then, the light detected at the point $\mathbf{r}_d$ at the boundary is the outward flux of diffusing light and is given by the normal derivative of U evaluated at $\mathbf{r}_d$,

$$P(s) \propto -\hat{\mathbf{n}} \cdot \nabla U|_{\mathbf{r}_d} \ , \tag{15}$$

where $\hat{\mathbf{n}}$ is the unit normal vector, directed outward. It is the intensity of diffusing photons that satisfies the diffusion equation,

$$\frac{\partial U}{\partial t} = D_l \nabla^2 U \ , \tag{16}$$

where $D_l = cl^*/3$ is the diffusion coefficient for light. The geometry for the solution of the diffusion equation will depend on the experiment. As initial conditions for the diffusion equation, we take an instantaneous pulse at $t = 0$, with a geometry suitable for the experiment. The boundary conditions must ensure that there is no flux of diffusing photons entering the sample from the boundaries. This is achieved with the boundary conditions[15]

$$U - \frac{2}{3} l^* \hat{\mathbf{n}} \cdot \nabla U = 0 \ . \tag{17}$$

We use the transformation of variables, $s = ct$, to relate the time dependence to the required distribution in path lengths. We can then solve the Laplace transform of the diffusion equation, take its normal derivative at the surface and obtain the autocorrelation function directly.

Finally, to compare to experiment, we note that the electric field autocorrelation functions discussed above are usually not measured directly. Instead, one typically measures the intensity (or homodyne) autocorrelation function, $\langle I(\tau)I(0)\rangle/\langle I\rangle^2$, where I is the intensity of the scattered light. For most systems of experimental interest, the intensity autocorrelation function is simply related to the electric field autocorrelation function by

$$\langle I(\tau)I(0)\rangle/\langle I\rangle^2 = 1 + f(A)g_2(\tau) \ ,$$

where $f(A)$ is a function determined by the collection optics,[1,2] $g_2(\tau)$ is related to $g_1(\tau)$ by the Siegert relation,

$$g_2(\tau) = |g_1(\tau)|^2$$

and $g_1(\tau)$ is the normalized field autocorrelation function, $g_1(\tau) \equiv \langle E(\tau)E^*(0)\rangle / \langle |E|^2 \rangle$. The validity of the Siegert relation in the multiple scattering regime has been verified experimentally for $\tau = 0$, and no evidence for non-Gaussian statistics is found.[16] Experimental results are generally reported as normalized homodyne autocorrelation functions, $g_2(\tau)$.

3. TRANSMISSION

The first experimental geometry we consider is transmission through a slab of thickness L and infinite extent.[6,7] For the transmission geometry, the detected light must diffuse a distance L across the sample, as illustrated in the top of Fig. 3. This introduces a characteristic path length, $s_c = n_c l = n_c^* l^*$, where $n_c^* = (L/l^*)^2$ is the mean number of steps for a random walk of end-to-end distance L and average step length l^*. The consequences of this characteristic length can be seen directly in the dispersion induced in a delta function pulse upon traversal of a sample with $L = 1$ mm and $l^* = 100$ μm, illustrated in the bottom of Fig. 3. The intensity is peaked sharply and then decays rapidly with increasing time. Since this time dependence is proportional to $P(s)$, this characteristic path length will be directly reflected in the autocorrelation function resulting in a characteristic decay time. Physically, this corresponds to the time taken for the characteristic path length to change by $\sim \lambda$, so that the total phase $\Delta\phi^{(n^*)} \approx 1$. Thus, we can estimate the typical distance an individual particle has moved from the condition

$$\langle (\Delta\phi^{(n^*)})^2 \rangle \approx n_c \langle q^2 \rangle \langle \Delta r^2 \rangle \approx \left(\frac{n_c^* l^*}{l} \right) \left(2k_0^2 \frac{l}{l^*} \right) \langle \Delta r^2 \rangle \approx 1 \, .$$

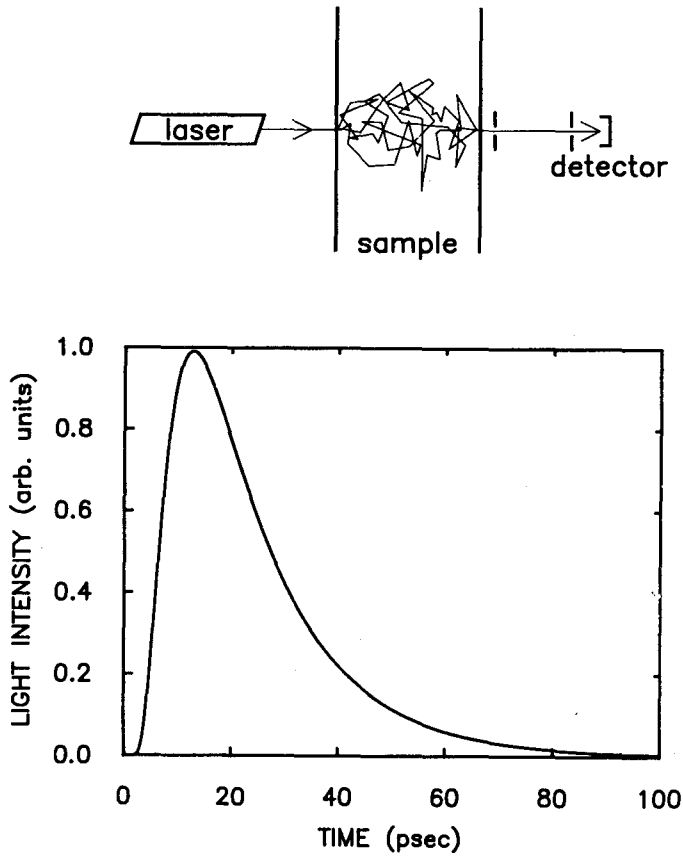

Fig. 3. Transmission of a short pulse of light through a multiply scattering medium: (top) Experimental geometry showing light paths which exit at a point directly opposite the input pulse. Other paths are present, but not shown; (bottom) Time-dependent output response to $\delta(t)$ input pulse ($L = 1$ mm, $l^* = 100$ μm, $c = 2 \times 10^{10}$ cm/s).

This gives $\Delta r_{\mathrm{rms}} \approx \lambda l^*/9L$. *Since* $l^*/L \ll 1$, *the typical length scale over which particle motion is probed by DWS in transmission is much smaller than the wavelength.* This reflects the fact that the decay of the autocorrelation function is due to the cumulative effect of many

scattering events, so that the contribution of individual particles to the total decay is small. *This is in striking contrast to ordinary dynamic light scattering (QELS) where by varying q, length scales greater than or equal to the wavelength are probed.* Furthermore, an important feature of the transmission geometry in DWS is that the length scale over which particle motion is probed can be controlled experimentally by varying the sample thickness L. Similarly, the time scale over which motion is probed using DWS can be controlled by varying the sample thickness. This time scale is $\tau_0(l^*/L)^2$, and is much shorter than the time scales probed using QELS, which are typically longer than τ_0. Thus, DWS provides a useful and convenient means for extending the length and time scales over which particle motion can be measured using dynamic light scattering techniques.

Autocorrelation functions measured in transmission are shown in Fig. 4 (Ref. 7). The sample consisted of 0.497 μm diameter spheres at a volume fraction of $\phi = 0.01$ in a 2.0 mm thick cuvette. There is no unscattered light transmitted through the sample, insuring that the strong multiple scattering limit is achieved. The data in the lower curve were obtained when the sample was illuminated uniformly by a 1-cm diameter beam from a 488 nm argon ion laser. Imaging optics collected the transmitted light from a 50 μm spot on the opposite side of the sample from a point near the center of the illuminated area. For comparison, the upper curve shows data obtained when the incident beam was focused to a point on one side of the sample and transmitted light was collected from a point on axis with the incident spot. These data clearly decay somewhat more slowly than the data obtained with an extended source illumination. Physically, this difference reflects the fact that for the extended source there is a larger contribution from long paths, resulting in a somewhat faster decay than for the point source.

To quantitatively analyze these data, we obtain $g_1(\tau)$ by solving the Laplace transform of the diffusion equation as previously discussed. We take the source of diffusing intensity to be a distance $z = z_0$ inside the illuminated face where we expect that $z_0 \sim l^*$. We first consider the

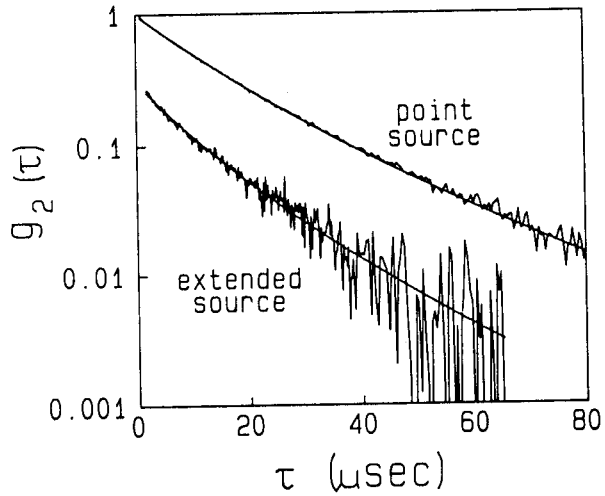

Fig. 4. Intensity autocorrelation functions *vs* time for transmission through 2-mm thick cells with 0.497-μm-diameter polystyrene spheres and $\phi = 0.01$. Smooth lines are fits to the data by Eqs. (15) and (16) with $l^* = 173$ μm for the point source and $l^* = 175$ μm for the extended source.

case of uniform illumination of one side by an extended source. From Eqs. (12) and (15), we obtain

$$g_1(\tau) = \frac{\frac{L+(4/3)l^*}{z_0+(2/3)l^*}\left\{\sinh\left[\frac{z_0}{l^*}\sqrt{\frac{6\tau}{\tau_0}}\right] + \frac{2}{3}\sqrt{\frac{6\tau}{\tau_0}}\cosh\left[\frac{z_0}{l^*}\sqrt{\frac{6\tau}{\tau_0}}\right]\right\}}{\left(1+\frac{8\tau}{3\tau_0}\right)\sinh\left[\frac{L}{l^*}\sqrt{\frac{6\tau}{\tau_0}}\right] + \frac{4}{3}\sqrt{\frac{6\tau}{\tau_0}}\cosh\left[\frac{L}{l^*}\sqrt{\frac{6\tau}{\tau_0}}\right]} \qquad (18a)$$

$$\approx \frac{\left(\frac{L}{l^*}+\frac{4}{3}\right)\sqrt{\frac{6\tau}{\tau_0}}}{\left(1+\frac{8\tau}{3\tau_0}\right)\sinh\left[\frac{L}{l^*}\sqrt{\frac{6\tau}{\tau_0}}\right] + \frac{4}{3}\sqrt{\frac{6\tau}{\tau_0}}\cosh\left[\frac{L}{l^*}\sqrt{\frac{6\tau}{\tau_0}}\right]}, \qquad (18b)$$

where the second expression holds for $\tau \ll \tau_0$. The characteristic time scale in these expressions is $\tau_0(l^*/L)^2$.

For the second geometry, we consider light incident from a point source on axis with the detector, and obtain

$$g_1(\tau) \propto \int_{(L/l^*)\sqrt{6\tau/\tau_0}}^{\infty} [A(s)\sinh s + e^{-s(1-z_0/L)}]ds\,, \qquad (19a)$$

where

$$A(s) = \frac{(\varepsilon s - 1)[\varepsilon s e^{-s z_0/L} + (\sinh s + \varepsilon s \cosh s) e^{-s(1-z_0/L)}]}{(\sinh s + \varepsilon s \cosh s)^2 - (\varepsilon s)^2} \tag{19b}$$

and $\varepsilon = 2l^*/3L$. For convenience, we take $z_0 = (4/3)l^*$, but note that the solutions are insensitive to the exact value used since, in general, $z_0 \sim l^*$ and $l^*/L \ll 1$. This reflects the fact that the value chosen for z_0 affects only the first few steps of a random walk which typically consists of a great number of steps. Thus, the relative contribution of the first few steps is small.

These expressions can be compared directly to the experimental data. In Fig. 4, the solid lines through the data are fits to the appropriate equations above. The time constant $\tau_0 \equiv (Dk_0^2)^{-1}$ is set equal to 3.73 msec where D was obtained from a QELS measurement in the single scattering limit at $\phi = 10^{-5}$. The diffusion coefficient D remains independent of concentration for the particle concentrations used in these measurements. For both cases, the data are well-described by the predicted forms of $g_2(\tau)$ with l^* the only fitting parameter. The fit gives $l^* = 175$ μm for the extended source and $l^* = 173$ μm for the point source. This excellent consistency for the fitted values of l^* confirms that the somewhat different decay rates in Fig. 4 are due solely to geometric effects. The values of l^* compare well with Mie theory which gives a value of $l^* = 195$ μm, about 10% higher than measured. This small difference may be due to the approximate nature of the boundary condition on the exit side. Indeed, a slightly smaller value for l^* was obtained in an earlier analysis of this data, which used different boundary conditions, demonstrating the sensitivity of $g_1(\tau)$ to the boundary conditions.

While the autocorrelation functions shown in Fig. 4 are clearly not single exponentials, their curvature in the semi-logarithmic plot is not large. This reflects the existence of a dominant characteristic path length and time scale for these data, as expected. This also suggests the suitability of analyzing the data by means of the first cumulant Γ_1,

or the logarithmic derivative at zero time delay. For Eq. (18), the first cumulant is given by

$$\Gamma_1 = \frac{\partial \ln g_1(\tau)}{\partial \tau}\Big|_{\tau=0} \approx \frac{(L/l^*)^2 + 4(L/l^*) + 8/3}{\tau_0(1 + 4l^*/3L)} \,. \tag{20}$$

For Eq. (19), the first cumulant must be evaluated numerically. Measurements of $\sqrt{\Gamma_1}$ as a function sample thickness are shown in Fig. 5 for several volume fractions. The plots show the expected linear dependence of $\sqrt{\Gamma_1}$ over a broad range of concentrations confirming the diffusive nature of the transport of light. It is apparent that the data do not extrapolate through the origin but that the x-intercepts are a monotonically decreasing function of particle concentration and, to within experimental uncertainty, consistent with Eq. (20). The different slopes are due primarily to the concentration dependence of l^*, which is expected to scale inversely with particle density.

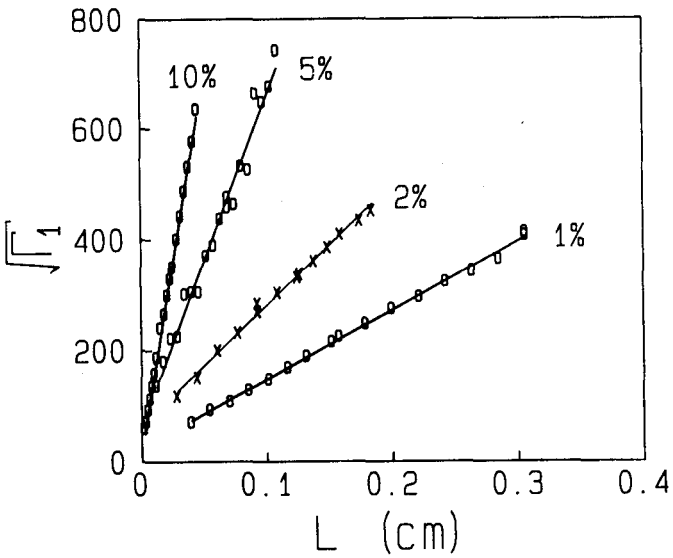

Fig. 5. Square root of the first cumulant Γ_1 *vs* sample thickness L for 0.497-μm-diameter spheres for different volume fractions ϕ.

4. BACKSCATTERING

Another interesting and important geometry is that of backscattering.[4,5,6,7] Here, the light is incident uniformly on one face of a slab of thickness, L, and the scattered light is collected from the same face, as illustrated at the top of Fig. 6. In contrast to transmission, in backscattering there is no well-defined characteristic path length set by the sample thickness. This can be seen from the time dependence of the detected intensity of an incident delta function pulse, shown at the bottom of Fig. 6. The intensity is peaked at early times, corresponding to the fact that most of the light is scattered back after only a few scattering events. However, there is still considerable light detected at larger times, as reflected by the very slow decay of the intensity as t increases. To emphasize this point, it is instructive to contrast the behavior of backscattered light with that of transmitted light. We do this in Fig. 7, which shows the dispersion induced in delta function pulses for transmission (dashed line) and backscattering (solid line), plotted logarithmically. The transmission pulse is sharply peaked at the time corresponding to the characteristic path length, and decays rapidly at later times. By contrast, the backscattered pulse is peaked at very early times, corresponding to the light immediately backscattered, but then has a very long, power-law decay. In Fig. 7, we also show on the upper axis the number of scattering events, n^*, corresponding to the transit time, t.

This power-law decay in the dispersion of a delta function pulse is directly reflected in $P(s)$ for the backscattering geometry. As a result, the autocorrelation function no longer depends sensitively on l^*, and, in principle, it becomes possible to determine τ_0 without prior knowledge of l^*. In fact, since paths of all lengths contribute in backscattering, the autocorrelation function consists of contributions from all orders of multiple scattering. As a consequence, there is a much broader distribution of time scales in the decay. The longer paths consist of a larger number of scattering events and thus decay more rapidly, probing the

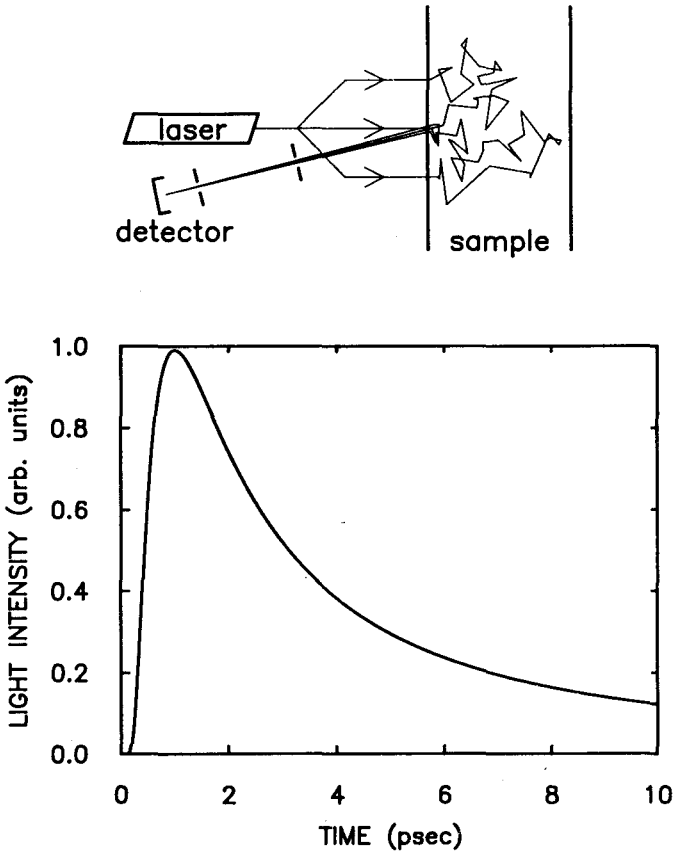

Fig. 6. Backscattering of a short pulse of light from a multiply scattering medium. Input beam is expanded and columated; light is detected near the center of the area illuminated by the input pulse. (top) Experimental geometry showing light paths which exit at a point directly opposite the input pulse. Other paths are present, but not shown. (bottom) Time-dependent output response to $\delta(t)$ input pulse ($L = 1$ cm, $l^* = 100$ μm, $c = 2 \times 10^{10}$ cm/s, $z_0 = 2l^*$).

motion of individual particles over shorter length and time scales. By contrast, the shorter paths consist of a smaller number of scattering events thus decaying more slowly and probing the motion of individual particles over longer length and time scales. This feature is particularly

advantageous for exploring the dynamics of interacting systems, which can have a broad distribution of relaxation rates associated with motion over different lengths scales.

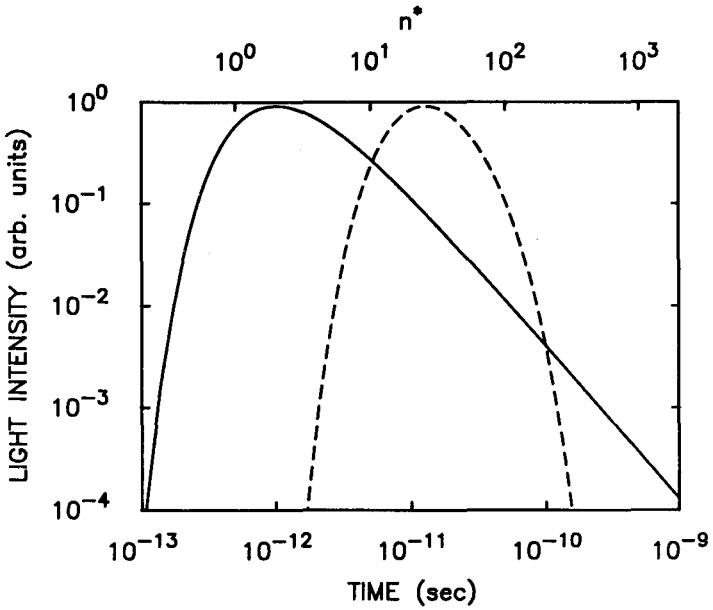

Fig. 7. Comparison of $I(t) \propto P(s)$ for backscattering (solid line) and transmission (dashed line) geometries.

To derive a functional form for the autocorrelation function for backscattered light, we consider a slab of thickness, L, and of infinite extent, uniformly illuminated from one side (Fig. 6). While we would like to maintain the simplicity and elegance of the Laplace transform approach used in the case of transmission, we must be extremely cautious in using this for backscattering. In obtaining the Laplace transform in Eq. (12), we have used a continuum approximation to change the summation paths in Eq. (11) to an integral. However, since $s = nl$ and we must have at least one scattering event, we require $n \geq 1$; thus, the lower bound on s must be l rather than 0. Equivalently, for isotropic scatterers, where $l = l^*$, the decay time for a path of length s is

$\exp[-(2\tau/\tau_0)s/l]$. Allowing $s < l$ leads to unphysically long decay tim since $\tau_0/4$ represents the shortest decay time possible, corresponding light singly scattered through 180°. Similarly, for anisotropic scatter where $l^* > l$, we require $s \geq l^*$ to obtain physically meaningful dec times. However, in order to maintain the simplicity of the Lapla transform, the lower bound on the integral must be zero. For transmi sion, this does not present a problem as the shortest possible paths a $s = L$, so that $n \gg 1$. By contrast, for backscattering, short paths d contribute and thus, in using the diffusion approximation, we must e sure that the contribution of the unphysically short paths is suppresse

A simple way of achieving this is to solve the diffusion equati using an initial condition of a source at a fixed distance, z_0, in from t illuminated face at $z = 0$. This ensures that there are no contributio from paths shorter than z_0. Physically we can regard this as the sour of the diffusing intensity, which we expect to be peaked at $z_0 \sim l$ Thus, for the initial condition we take $U(\mathbf{r}, t = 0) = \delta(x, y, z - z_0)$ and for the boundary conditions again we use Eq. (17). The soluti for this geometry is,

$$G_1(\tau) = \frac{\sinh\left[\sqrt{\frac{6\tau}{\tau_0}}\left(\frac{l}{l^*} - \frac{z_0}{l^*}\right)\right] + \frac{2}{3}\sqrt{\frac{6\tau}{\tau_0}}\cosh\left\{\sqrt{\frac{6\tau}{\tau_0}}\left(\frac{L}{l^*} - \frac{z_0}{l^*}\right)\right\}}{\left(1 + \frac{4}{9}\frac{6\tau}{\tau_0}\right)\sinh\left[\frac{L}{l^*}\sqrt{\frac{6\tau}{\tau_0}}\right] + \frac{4}{3}\sqrt{\frac{6\tau}{\tau_0}}\cosh\left[\frac{L}{l^*}\sqrt{\frac{6\tau}{\tau_0}}\right]} . \quad (2$$

For a sample of infinite thickness, Eq. (21) simplifies,

$$G_1(\tau) = \frac{e^{-(z_0/l^*)\sqrt{6\tau/\tau_0}}}{1 + \frac{2}{3}\sqrt{\frac{6\tau}{\tau_0}}} . \quad (2$$

We note that the initial condition of a source at z_0 appears explicitly the solution, reflecting the importance of the contribution of the sh paths. In fact, we expect there to be a distribution in the position of apparent source, z_0. Thus we must integrate Eq. (22) over a distribut of sources, $f(z_0)$. While the exact form of $f(z_0)$ is unknown, we do kn that $f(z_0)$ goes to zero as $z_0 \gg l^*$ and for $z_0 \ll l^*$. Furthermore,

expect $f(z_0)$ to be peaked near $z_0 \sim l^*$. Thus, to leading order in $\sqrt{\tau/\tau_0}$, $g_1(\tau)$ is given by Eq. (22), with z_0/l^* replaced by $\langle z_0\rangle/l^*$, the average over the source distribution $f(z_0)$. The first order correction is $[\langle z_0^2\rangle/\langle z_0\rangle^2 - 1]\tau/\tau_0$ which is small for a narrow distribution $f(z_0)$. Physically, we can think of $\langle z_0\rangle$ as the average position of the source of diffusing intensity, and we expect that the exact form of the distribution $f(z_0)$, and therefore $\langle z_0\rangle$, will depend on the anisotropy of the scattering as reflected by l^*/l.

An autocorrelation function measured in backscattering is shown in Fig. 8. The sample consisted of 0.412 μm diameter spheres at a volume fraction of $\phi = 0.05$ in a 5 mm thick cuvette. It was illuminated by a uniform beam, 1 cm in diameter; light from a 50 μm diameter spot near the center of the illuminated area was imaged onto the detector. The scattering angle was $\sim 175°$, although we found virtually no dependence of the results on scattering angle when it was varied $\sim 20°$ from that used here. This is expected for diffusing light. After subtracting the baseline, the logarithm of the autocorrelation function, normalized by the baseline is plotted as a function of the square root of time, in units of τ_0. We use $\tau_0 = 3.01$ msec, as measured experimentally in the single scattering limit, and consistent with the value calculated from the Stokes-Einstein relation. The solid line is a fit to the functional form given by Eq. (22), and is in reasonably good agreement with the data. However, the theoretical form exhibits somewhat more curvature than the data. In fact, to within the precision of experiment, the data shown in Fig. 8 is linear over three decades of decay when plotted logarithmically as a function of the square root of time. This suggests that the data can be more simply described using

$$G_1(\tau) = e^{-\gamma\sqrt{6\tau/\tau_0}}\ , \tag{23}$$

where $\gamma = \langle z_0\rangle/l^* + 2/3$. This result was obtained previously using the simpler, but less rigorous, boundary condition, $U(z = 0) = 0$ (Refs. 7,8).

The behavior of the autocorrelation function shown in Fig. 8 is in fact quite general. Virtually all the autocorrelation functions that

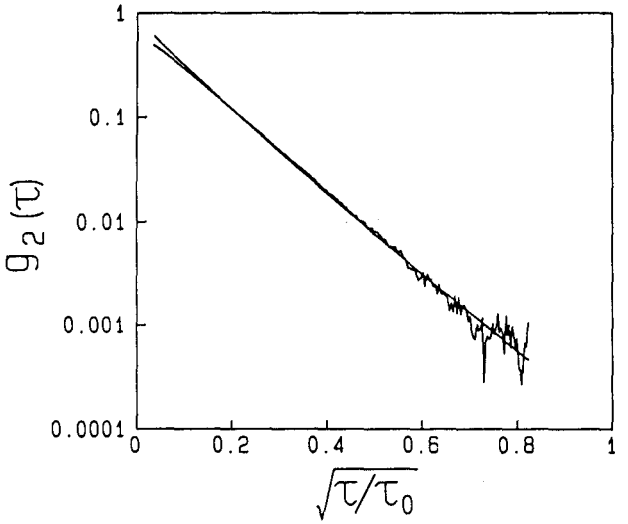

Fig. 8. Intensity autocorrelation function *vs* sqaure root of reduced time for backscattering from a 5-mm thick cell with 0.412-μm-diameter polystyrene spheres and $\phi = 0.05$. The line through the data is a fit to the theory in Eq. (22), and has a more rapid initial decay and more curvature than the data.

we have measured in backscattering for freely diffusing particles exhibit a similar behavior in that they decay exponentially in the square root of time. Therefore, it is most convenient to use the very simple form in Eq. (23) to describe their shape. The slope of the autocorrelation function, when plotted in this fashion, is determined solely by τ_0 and by γ. While we have derived this functional form using rather heuristic arguments, similar results are also obtained using more rigorous diagrammatic techniques.[18] However, it is again essential to properly account for the contributions of the short paths. This can be done by ensuring that the difference between initial and final wavevectors is strictly $2k_0$, as required for backscattering, and by limiting the momentum transfer in any single scattering event to properly reflect the form factor of the scatterers. By contrast, if this is not done, the contributions of the short paths are over estimated in the diagrammatic

approach, leading to a prediction[6] for the autocorrelation function that describes the initial decay reasonably well, but fails at longer times by predicting a power-law decay, in sharp disagreement with the data.

Using samples of known τ_0, we find experimentally that γ depends on both polarization and on the anisotropy of the scattering, as characterized by l^*/l. The dependence of γ on polarization is strongest for isotropic scatterers, when $l^*/l \to 1$, as illustrated by the data in Fig. 9a. These data are obtained from a $\phi = 0.02$ sample of 0.091 μm diameter spheres, for which $l^*/l \approx 1.1$. The sample is illuminated by linearly polarized light, and an analyzer is used to detect scattered light whose polarization is either parallel or perpendicular to the incident light. The autocorrelation function for the perpendicular polarization decays more rapidly, because the analyzer discriminates against the low order paths which retain a high degree of their incident polarization. This reflects the contribution of multiple scattering paths for which the diffusion approximation is more appropriate. The value measured is $\gamma = 2.5$. By contrast, the autocorrelation function for the parallel polarization decays more slowly, because of the additional contribution of the low order scattering paths which have a longer decay time. We note, however, that the form of the autocorrelation function is still the same, remaining linear when plotted exponentially as a function of the square root of time. Here, the value measured is $\gamma = 1.6$. By contrast, for very anisotropic scatterers, the dependence of γ on polarization is very weak. This is illustrated in Fig. 9b, which shows data obtained using a $\phi = 0.02$ sample of 0.605 μm diameter spheres, for which $l^*/l \approx 10$. The autocorrelation function for the perpendicular polarization again decays faster, with $\gamma_\perp = 2.1$; for the parallel polarization, $\gamma_{||} = 2.0$.

We summarize the dependence of γ on l^*/l for both polarizations in Fig. 10. The data are obtained by varying the size of the spheres to vary l^*/l, since for the particle sizes used here this ratio is a monotonic function of sphere diameter. In all cases, $\phi = 0.02$. The data suggests that, for each polarization, γ asymptotically approaches a constant as l^*/l becomes large. Physically, this reflects the diminishing contribu-

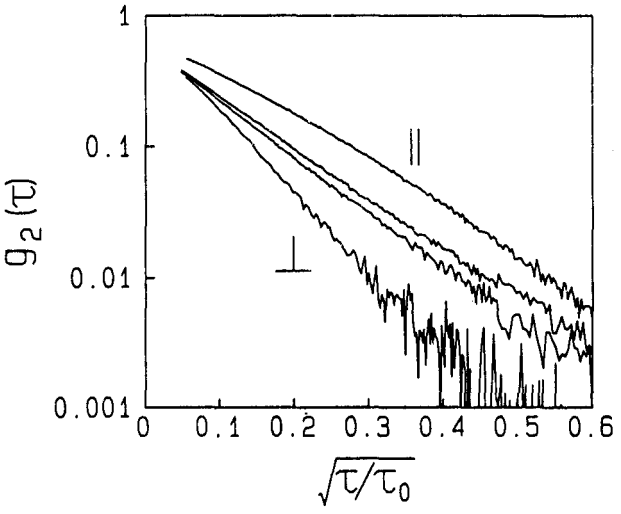

Fig. 9. Intensity autocorrelation functions *vs* square root of reduced time for backscattering for parallel and perpendicular polarizations. The upper and lower curves are for 0.091-μm-diameter spheres, with $\gamma_{\|} = 1.6$ and $\gamma_{\perp} = 2.9$; the two middle curves are for 0.605-μm-diameter spheres, with $\gamma_{\|} = 2.0$ and $\gamma_{\perp} = 2.1$.

tions of the short paths as the scattering becomes more strongly peaked in the forward direction. In this case, the diffusion approximation, which is scalar in nature, should apply. Therefore, $g_1(\tau)$ becomes a function of τ/τ_0 only, and thus, in this limit, γ does not depend on l^*/l. In fact, an asymptotic value of $\gamma = 2.1$ is predicted theoretically by properly considering the contribution of the short paths to the autocorrelation function at long times.[18,19] Furthermore, the trends observed in Fig. 10 for the dependence of γ on both l^*/l and polarization are consistent with the predictions made using diagrammatic techniques.

The variation of γ with particle size arises from the contributions of short paths, which are different for different polarizations and values of l^*/l. By contrast, the *absolute* decay of the unnormalized autocorrelation function, $G_1(\tau)$, at short times is due solely to the contributions of *long paths* which are well described within the diffusion

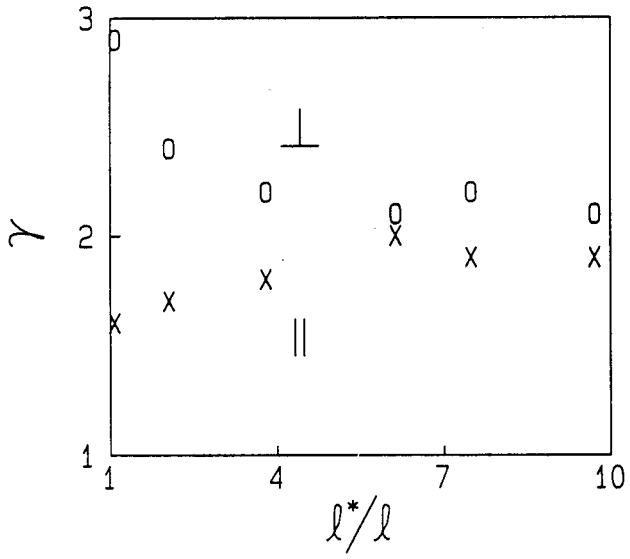

Fig. 10. Experimental values of γ *vs* l^* / l and particle size for parallel (cross and perpendicular polarizations (circles).

approximation. These contributions should be independent of polari tion and l^*/l due to the large number of scattering events. This le to an important relation between the value of γ and the static intens $G_1(0) \equiv \langle |E|^2 \rangle = \langle I \rangle$. To see this, we examine the short time expans for $G_1(\tau)$ for a semi-infinite sample,

$$G_1(\tau) = G_1(0) - \gamma G_1(0)\sqrt{\frac{6\tau}{\tau_0}} + \dots \ .$$

The characteristic square root of time dependence arises from the c tributions of long paths and is independent of the boundary and init conditions assumed. The rate of the *absolute* decay, $\partial G_1(\tau)/\partial\sqrt{\tau/\tau_0}$ also determined solely by the long paths. Thus, the coefficient, $\gamma G_1($ should be a constant independent of polarization and l^*/l. Hence, si $G_1(0) = \langle I \rangle$ we expect

$$\gamma \propto \frac{1}{\langle I \rangle} \ .$$

This implies that both γ and $\langle I \rangle$ depend on the contributions of low order scattering and on the sample used. Physically, we expect $\langle I \rangle$ to decrease for large l^*/l or for perpendicular polarization, both of which reduce the number of short paths contributing to the scattered intensity. Similarly, we expect γ to increase when the contributions of short paths are reduced since it is the short paths which have the longest decay times.

To test these ideas, we again consider the behavior of the experimental autocorrelation function $g_2(\tau) = |g_1(\tau)|^2$. Figure 11 shows a plot of $g_2(\tau)$ *vs* $\sqrt{\tau/\tau_0}$ obtained using an extended light source with parallel polarizer and analyzer.[11] The measurements were taken using four different diameters of polystyrene spheres: 0.102 μm, 0.305 μm, 0.46 μm, and 0.797 μm. In each case, the sample size was 1cm $\times$ 1cm $\times$ 1cm and the volume fraction of spheres was $\phi = 0.10$. The autocorrelation function, $g_1(\tau)$, appears to have the same form as a function of τ/τ_0 for the three larger size spheres studied. Since the static average intensity $\langle I \rangle$ turns out to be the same for these samples, it is also consistent with the prediction that the coefficient $\gamma G_1(0)$ is constant. The autocorrelation function $g_2(\tau)$ decays slightly more slowly for the smallest beads, again consistent with the slightly larger static intensity observed in this case. Finally, the inset in Fig. 11 shows that the initial decay of the autocorrelation function is linear in $\sqrt{\tau/\tau_0}$, as expected from Eq. (23).

5. ANALOGIES WITH STATIC MEASUREMENTS

The functional form of the temporal autocorrelation function depends crucially on the distribution of paths explored by the diffusing light. In backscattering, $g_1(\tau)$ is particularly sensitive to the contributions of short paths as evidenced by the dependence of γ on polarization and l^*/l. Thus, measurements of $g_1(\tau)$ become a sensitive probe of the nature of the transport of light when there is significant multiple scattering. Other optical properties of strongly scattering media also depend on $P(s)$: the angle (q) dependence of the coherent enhancement of the

backscattering cone and the absorption dependence of the incoherent backscattered intensity. In fact, within the diffusion approximation, the description of all three of these quantities depends on $P(s)$ in exactly the same way. The analogy that exists between these three quantities dramatically illustrates the similarity of the underlying physics and the utility of the diffusion approximation in describing a wide variety of multiple scattering processes. The analogy also has practical consequences: it leads to a way of experimentally determining γ, and therefore also τ_0, without recourse to any specific theory about the distribution of the low order multiple scattering paths which are not rigorously described within the diffusion approximation.

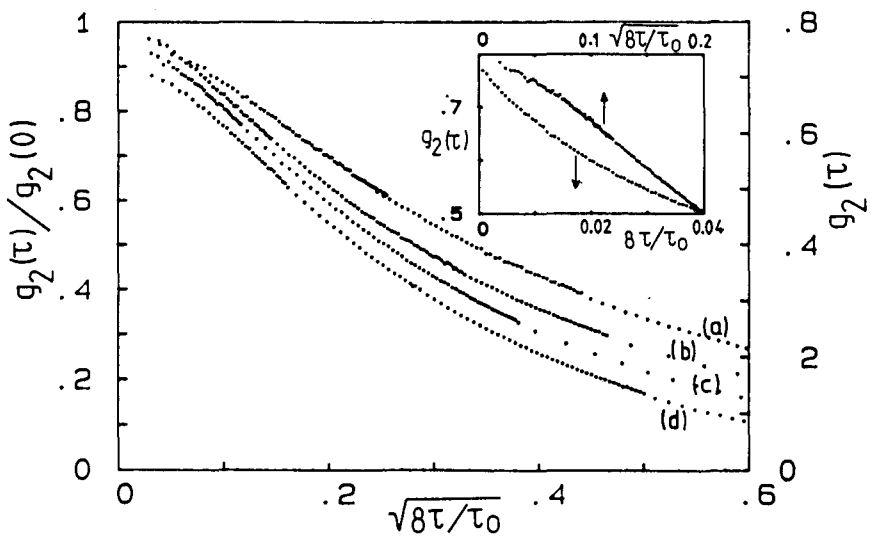

Fig. 11. Intensity autocorrelation functions *vs* reduced time for backscattering for polystyrene spheres of various diameters and $\phi = 0.10$. The inset shows that the initial decay is linear in the square root of time.

We have already considered the temporal autocorrelation function in the previous section where we found that for $\tau/\tau_0 \ll 1$,

$$\frac{G_1(\tau)}{G_1(0)} = 1 - \gamma\sqrt{\frac{6\tau}{\tau_0}} + \cdots , \tag{24}$$

where the coefficient $\gamma G_1(0)$ does not depend on the contributions of short paths.

Next, we consider the coherent backscattering cone. As outlined elsewhere in this volume, the average scattered intensity is higher in the backward direction than at wide angles. This is because for each scattering path there exists a time-reversed path of identical length which contains the same fraction of the total intensity and has the same phase shifts. Light emerging from both of these paths interferes constructively in the backward direction. The angular dependence of this coherent enhancement above the incoherent wide angle intensity is controlled by the spatial separation of the endpoints of the path, ρ. The enhancement for a given angle and a given path length s is simply the Fourier transform of the probability distribution $p(\rho, s)$

$$\alpha(s, q_0) = I_0 \int p(\rho, s) e^{-\mathbf{q}_0 \cdot \boldsymbol{\rho}} d^2\rho \propto P(s) e^{-q_0^2 l^* s/3} \ ,$$

where $\mathbf{q}_0$ is the scattering vector with respect to the backscattering angle ($\theta_0 = 0$) and its magnitude is $q_0 = 4\pi n/\lambda \sin(\theta_0/2)$. This means that the paths of length s, which have a mean square end-to-end distance of $\sim \sqrt{sl^*}$, contribute a gaussian of angular width $\lambda/\sqrt{sl^*}$ and of amplitude $P(s)$ to the total coherent backscattering enhancement $\alpha(q_0)$ [albedo]. Thus, $\alpha(q_0)$ is obtained by integrating over these Gaussians,

$$\alpha(q_0) \propto \int P(s) e^{-q_0^2 l^* s/3} ds \ . \tag{25}$$

Equation (25) has the same form as Eq. (12) when the identification $2\tau/\tau_0 \rightarrow (ql^*)^2/3$ is made. Therefore, by analogy the angular variation of $\alpha(q_0)$ at small $q_0 (q_0 l^* \ll 1)$ is given by

$$\frac{\alpha(q_0)}{\alpha(0)} = 1 - \gamma q l^* + \dots \ , \tag{26}$$

where the coefficient γ is the same as in Eq. (24) for the same sample, provided that single scattering is negligible.[11] The square root singularity of $G_1(\tau)$ with time maps into a linear singularity of $\alpha(q_0)$ with angle.

We can also compare $G_1(\tau)$ and $\alpha(q_0)$ with the dependence on absorption of the incoherent intensity near backscattering. If the absorption in the scattering medium is characterized by an absorption length, l_a, then the fraction $P(s)$ of the intensity scattered on average along a path of length s is attenuated by $\exp(-s/l_a)$. The total scattered intensity can then be written as an integral over the distribution of path lengths,

$$\alpha_I(l_a) \propto \int P(s) e^{-s/l_a} ds \; . \tag{27}$$

This form also maps into $G_1(\tau)$ and $\alpha(q_0)$ in Eqs. (12) and (25) when the identifications $2\tau/\tau_0 \rightarrow (ql^*)^2/3 \rightarrow l^*/l_a$ are made. Therefore, the variation of the normalized backscattered intensity with absorption for weak absorption ($l^* \ll l_a$) bceomes

$$\frac{\alpha_I(l_a)}{\alpha_I(\infty)} = 1 - \gamma\sqrt{\frac{3l^*}{l_a}} + \ldots \; . \tag{28}$$

Equations (24), (26), (28) are three equivalent relations for the initial slope of the normalized temporal autocorrelation function, the normalized angular dependence of the coherent backscattering cone, and the normalized dependence of the incoherent scattering intensity on absorption. These equations contain essentially three potentially unknown parameters: γ, τ_0, and l^*. Thus in principle, an absolute measure of a particle's diffusion coefficient D can be obtained from τ_0 by experimentally determining $g_1(\tau), \alpha(q_0)/\alpha(0)$, and $\alpha_I(l_a)/\alpha_I(\infty)$ on the same sample in the short time, small angle, and weak absorption regimes, respectively. Physically, this correspondence reflects the fact that all these processes probe the same long diffusion paths of the light. This analogy demonstrates the simplicity and power of the diffusion approximation in treating the consequences of multiple scattering.

We demonstrate this correspondence in Fig. 12. We compare the temporal decay of $g_2(\tau)$ plotted as a function of $\sqrt{\tau/\tau_0}$ with the variation of the static incoherent intensity $\langle I \rangle$ as a function of added absorbing dye for a $\phi = 0.10$ suspension of 0.46 μm diameter spheres.[11] We

find good agreement with Eqs. (24) and (28). Even beyond the linear regime the two quantities show a very similar functional dependence when plotted as a function of the appropriate variables, $\sqrt{2\tau/\tau_0}$, and $\sqrt{l^*/l_a}$. This demonstrates the validity of Eq. 12. In fact, the value of τ_0 used in order to achieve good matching between the two data set is 10% larger than the free particle diffusion time in backscattering. This could be due to a slight reduction of D which is expected because of the hydrodynamic interactions between particles.

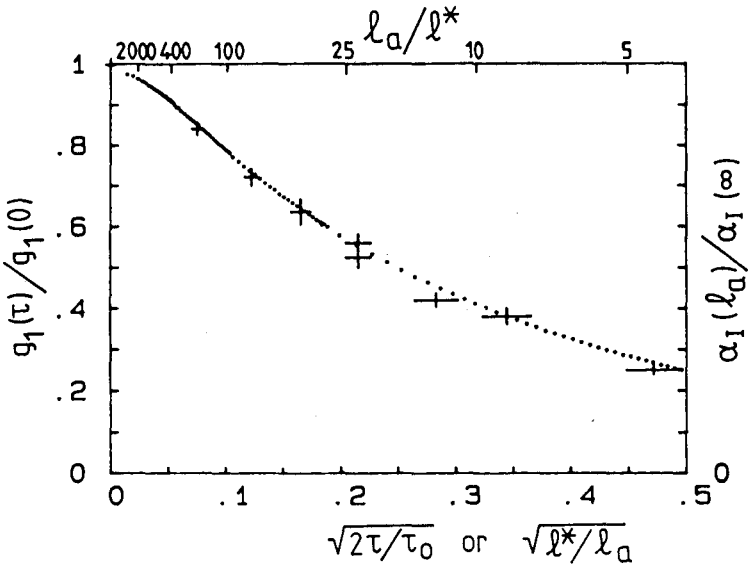

Fig. 12. Comparison of the temporal autocorrelation function *vs* $\sqrt{2\tau/\tau_0}$ with the incoherent intensity *vs* $\sqrt{l/l_a}$ for backscattering from 0.46-μm-diameter spheres with $\phi = 0.10$.

6. APPLICATIONS

In the previous sections we limited our theoretical treatment of the autocorrelation function of multiply scattered light to non-interacting, monodisperse particles whose dynamics were determined solely from their Brownian motion. In this section we generalize our treatment to

investigate the behavior of the correlation function for other situations, including polydispersity in the particle size, absorption of light, and convective motion of the suspension. We also discuss the application of DWS to suspensions where interparticle interactions become important.

6.1. Particle Sizing

One of the most useful applications of DWS is for sizing particles.[4,8] In principle, we can combine DWS with measurements of the back-scattering cone or dependence on absorption to uniquely measure τ_0 for an unknown sample. In practice, it is more straightforward to exploit the features of DWS alone for particle sizing. To demonstrate the utility of DWS, we measured autocorrelation functions in backscattering with perpendicular polarization for monodisperse suspensions of polystyrene spheres of different diameters. In Fig. 13, we have plotted $\log g_2(\tau)$ *vs* $\sqrt{\tau/\tau_0}$ for six different samples with $\phi = 0.05$ and with sphere diameters, d, ranging from 0.091 μm to 0.605 μm. For $d \geq 0.3\mu$m, the scaled autocorrelation functions all fall on nearly the same curve, suggesting that the parameter $\gamma_\perp$ approaches a single value for large particle sizes. This is consistent with the data in Fig. 9 which show $\gamma_\perp$ saturating at a value of approximately 2.1 for large l^*/l. Thus, in the limit of large particle diameters, DWS can be used to unambiguously determine $\tau_0 = (Dk_0^2)^{-1}$. If the relationship between D and d is known, as it is for small ϕ, DWS can be used to determine particle diameter to better than 10%.

For $d < 0.3$, $\gamma_\perp$ is no longer independent of particle size but steadily increases with decreasing particle size. Since $\gamma_\perp$ and τ_0 enter the expression for the autocorrelation function multiplicatively, τ_0 cannot be obtained in a single measurement without prior knowledge of $\gamma_\perp$. However the data shown in Fig. 9 suggest that $\gamma_\perp/\gamma_\parallel$ is a monotonic function of l^*/l. Therefore, it is possible to unambiguously determine τ_0 using DWS for a given sample by measuring the autocorrelation functions for the different polarizations. In this case, the ratio of the decay rates gives the value of l^*/l allowing the absolute values of $\gamma_\perp$ and $\gamma_\parallel$

to be determined. Once $\gamma_\perp$ and $\gamma_\parallel$ are known, τ_0 can be obtained from the rate of decay of the autocorrelation function.

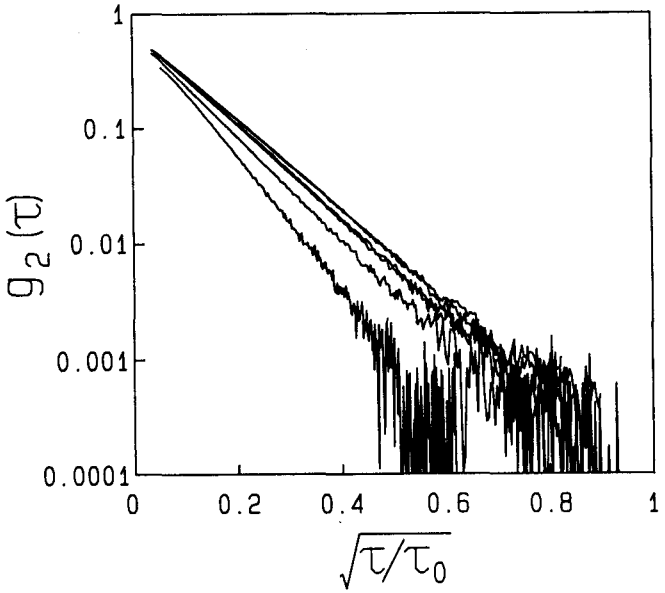

Fig. 13. Intensity autocorrelation functions *vs* square root time for backscattering for polystyrene spheres for six different samples with $\phi = 0.05$. From the lower left to the upper right corners, the curves correspond to data from spheres with the following diameters: 0.091 μm, 0.198 μm, 0.305 μm, 0.497 μm, 0.412 μm, 0.605 μm.

However, care must be exercised in using this scheme since the theory accounts only for the variations of γ arising from the single particle form factor, $F(\mathbf{q})$, and ignores the effects of longer range correlations as measured by the static structure factor, $S(\mathbf{q})$. As outlined below, estimates of the influence of $S(\mathbf{q})$ suggest that these effects may be significant at particle volume fractions as low as 10%. Fortunately, there are alternative methods for determining γ which do not depend on specific assumptions made about the details of the scattering properties of the medium. One of these methods depends on the analogy between DWS, coherent backscattering, and incoherent absorption discussed in

the previous section. However, this method requires that three independent measurements be made. An alternative, which is significantly simpler to implement, is to exploit the result that $\gamma\langle I\rangle$ should be a constant, independent of particle size. Thus, the diffusion coefficient D could be measured by comparing the decay of $g_2(\tau)$ to that of a calibration sample made up of polystyrene spheres with a known D. The ratio of the slope $\partial \ln g_2(\tau)/\partial\tau = \gamma\sqrt{6/\tau_0}$ times the ratio of the static intensities would provide the inverse ratio of $\sqrt{\tau_0}$ for the two different systems. In this way, the dynamics of concentrated suspensions could be probed and particle size could be determined provided, once again, that the relationship between D and d is known.

6.2. Polydispersity

We now consider the effects of polydispersity on the correlation function. In this case, the scattering medium possesses a distribution of species with different optical properties and different diffusion coefficients. In the case of conventional quasi-elastic light scattering, this leads to a non-exponential relaxation of the autocorrelation function. A considerable amount of research has gone into analysing the QELS data, to invert the shape of the non-exponential autocorrelation function and obtain information about the distribution of scattering species.[20] In the case of strong multiple scattering, the decay of the autocorrelation function is already non-exponential and geometry dependent. Should we then expect additional changes in the decay of the autocorrelation function due to the effects of polydispersity?

In the previous sections we have seen that the correlation function could be calculated if we knew the temporal dependence of the dephasing of a statistical path of n steps. The dephasing occurs by a random walk of phase shifts caused by the motion of the individual particles along the scattering path. For a polydisperse system the scattering from different size particles leads to phase shifts of different average magnitude resulting from the dependence of $\langle q^2\rangle$ and D on the particle diameter. This results in a random walk with different step sizes: In

the continuum limit, or diffusion approximation, the statistics of the random walks reduce to simple Gaussian functions. Thus, if the step size of a random walk varies for each step, then for large n, the statistics still remain the same as for a walk with a single average step size. This is the result of the central limit theorem. Thus, the time dependence of the autocorrelation function should be the same for a polydisperse system as for a monodisperse system. In contrast to QELS, there should be no additional information about polydispersity in these measurements. We will only measure average properties. The question which remains is how to calculate the appropriate average diffusion constant for a polydisperse sample.

Intuitively the answer is clear: We would expect the average diffusion constant to be weighted by the relative concentration of a species and by its scattering strength as expressed by its scattering cross section. As we detail below the intuitive answer is correct. We limit our discussion here to the case of non-interacting particles. For simplicity and illustration we first consider the case of a bimodal distribution, a density ρ_j of particles with scattering cross section σ_j and diffusion constant D_j, where $j = a, b$. We then replace Eq. (2) for the total phase shift for an nth order scattering process by

$$\Delta\phi^{(n)}(\tau) = \sum_{i=1}^{n} \mathbf{q}_i \cdot \Delta\mathbf{r}_i(\tau) = \sum_{i=1}^{n_a} \mathbf{q}_{a_i} \cdot \Delta\mathbf{r}_{a_i}(\tau) + \sum_{i=1}^{n_b} \mathbf{q}_{b_i} \cdot \Delta\mathbf{r}_{b_i}(\tau) \ , \quad (29)$$

where $n_a + n_b = n$. Since the average scattering wavevectors and rms displacements differ for the two species it is convenient to sum separately over the phase shifts for each species. The ensemble averages are calculated as in the monodisperse case but now keeping track of the species. Equation (5) becomes

$$G_1^{(n)}(\tau) = I_0 P(n) \left\langle e^{-q^2\langle \Delta r_{a_i}^2(\tau)\rangle/6} \right\rangle_q^{n_a} \left\langle e^{-q^2\langle \Delta r_{b_i}^2(\tau)\rangle/6} \right\rangle_q^{n_b} \ .$$

Performing the individual averages as before, we have

$$G_1^{(n)}(\tau) = I_0 P(n) e^{-n_a 2k_0^2 (l_a/l_a^*) D_a \tau - n_b 2k_0^2 (l_b/l_b^*) D_b \tau} \ , \quad (30)$$

where we have left the characteristic decay times τ_{0a} and τ_{0b} in terms of the diffusion coefficients for each species and k_0. Thus, $\tau_{0j} = (D_j k_0^2)^{-1}$.

We must now determine the average number of scattering events from particles a and b in a path of total length s. The relative probabilities of scattering by a or b are proportional to their number densities and total scattering cross sections or inversely proportional to their individual mean free paths

$$n_a/n_b = (\rho_a \sigma_a / \rho_b \sigma_b) = l_b/l_a$$

or $n_a l_a = n_b l_b$. Substituting this into Eq. (30) gives

$$\Delta\phi^{(n)}(\tau) = n_a l_a 2k_0^2 (D_a/l_a^* + D_b/l_b^*)\tau$$

where $\Delta\phi^{(n)}(\tau)$ is the exponent of Eq. (30). The total path length is given by n steps with the actual mean free path of the system l' which includes scattering from both species.

$$1/l' = \rho_a \sigma_a + \rho_b \sigma_b = 1/l_a + 1/l_b$$

$$s = nl' = n_a l_a$$

since $n = n_a + n_b = n_a(1 + l_a/l_b)$. For use below we also note:

$$1/l_{\text{eff}}^* \equiv (1/l_a^* + 1/l_b^*) \, .$$

The final result for the time dependent dephasing from the two species is therefore:

$$\Delta\phi^{(n)}(\tau) = s2k_0^2 (D_a/l_a^* + D_b/l_b^*)\tau$$

which is simply proportional to s and τ as expected, and has the same form as the previously derived expression for a single species. Thus, the time dependence of the correlation functions will not change from the results for a single species provided we substitute the appropriate averages for l^* and τ_0. Writing the phase shift as:

$$\Delta\phi^{(n)}(\tau) = (s/l_{\text{eff}}^*)(\tau/\tau_{\text{eff}})$$

and generalizing to the case of many different species we have directly:

$$1/l^*_{\text{eff}} = \sum_j 1/l^*_j \tag{31a}$$

$$1/\tau_{\text{eff}} = k_0^2 D_{\text{eff}} \tag{31b}$$

$$D_{\text{eff}} = (\sum_j D_j/l^*_j)/(\sum_j 1/l_j) \; . \tag{31c}$$

The effective diffusion constant is the weighted average of the diffusion coefficients. Since $1/l^*_j = \rho_j \sigma_j$, the weighting factor is the number density times the cross section for transport scattering or alternatively the inverse mean free path. The expressions for τ_{eff} and l^*_{eff} in Eq. (31) can be directly substituted for τ_0 and l^* in the correlation functions previously described. To illustrate this behavior, we measured the autocorrelation function in both transmission and backscattering from a series of binary mixtures of 0.198 μm and 0.605 μm diameter polystyrene spheres. In all cases, the functional form of the data obtained from mixtures is identical to that obtained from a single species. As an example, in Fig. 14, we show the autocorrelation function obtained in backscattering from a mixture of $\phi = 0.02$ of 0.198 μm spheres and $\phi = 0.02$ of 0.605 μm spheres. The expected exponential decay in the square root of time is apparent. We also calculate $1/l^*_i = \rho_i \sigma_i \langle 1 - \cos\theta_i \rangle$ for each species using Mie theory, and D_i from the Stokes-Einstein relation. The solid line through the data is the calculated decay using the calculated values of D_{eff} and l^*_{eff} and assuming that $\gamma = 2.1$. The agreement is excellent. Similar agreement is obtained for mixtures with different ratios. These results are summarized in Fig. 15 where we compare the value of τ_{eff} determined experimentally from backscattering measurements with that calculated theoretically from D_{eff} and l^*_{eff}.

We conclude by again emphasizing that, unlike QELS, DWS cannot yield independent information about polydispersity. Instead, only average quantities can be determined. However, we can calculate the average quantities if the distribution is known which, in principle, can allow the effects of different possible distributions to be tested. One

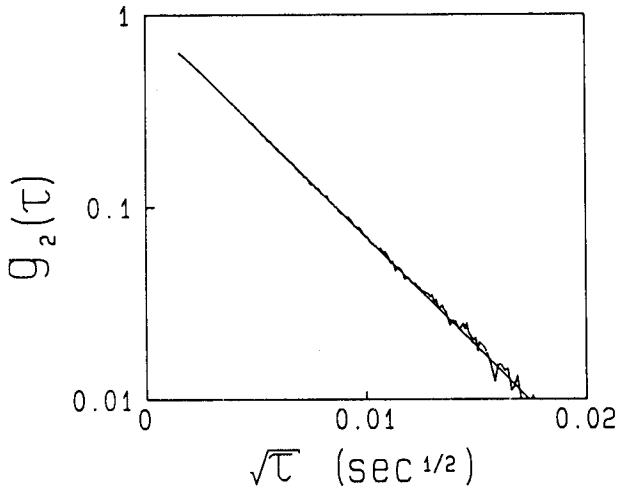

Fig. 14. Intensity autocorrelation functions *vs* square root reduced time for backscattering from a mixture with 0.198-μm-diameter spheres at $\phi_a = 0.02$ and 0.605-μm-diameter spheres at $\phi_b = 0.02$. The solid line through the data is determined without any fitting parameters using Eq. (31) as discussed in the text.

important effect that has not as yet been determined is the dependence of γ on polydispersity.

6.3. Porous Media

One application of the calculation for a polydisperse system is the limit where part of the sample consists of strong scatterers which are static while another component scatters and is diffusing. Such would be the case for particles diffusing in a porous medium. The result is straightforward, for the static components we simply set $D_j = 0$ in Eq. (31) and use the correlation functions previously described. For example if we have a porous structure with a transport mean free path l^* and we introduce a colloid which has the same l^* and a diffusion constant D (in the presence of the pores), then the correlation function would decay as for a homogeneous medium with effective diffusion constant $D/2$. The fact that the analysis of the data is so straightforward if we know the transport mean free paths of the porous structure

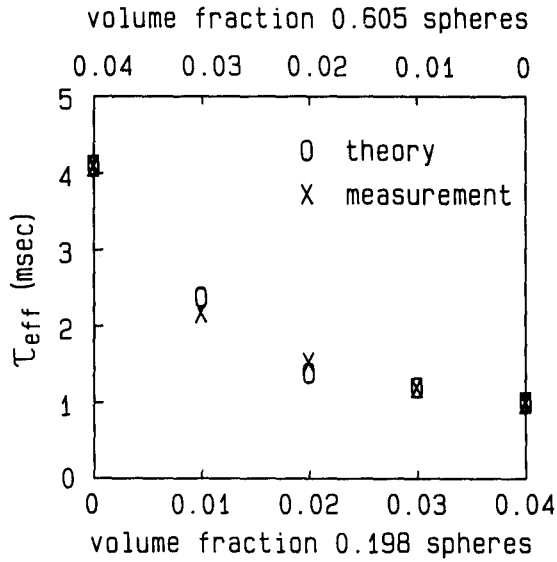

Fig. 15. Effective decay time τ_{eff} *vs* volume fraction ϕ for mixtures of 0.198-μm-diameter spheres and 0.605-μm-diameter spheres.

and the particles separately, implies that this should be a very useful way of seeing how the particle diffusion is affected by the presence of a confining geometry. To illustrate these ideas, in Fig. 16 we show an autocorrelation function obtained in backscattering from a glass frit with 4–8 μm diameter pores which were saturated with a $\phi = 0.01$ suspension of 0.497 μm diameter polystyrene spheres. The autocorrelation function exhibits the exponential decay in the square root of time. It is important to note that, in this case, the rigid glass frit provides a reference signal so that the autocorrelation function was measured in the *heterodyne* mode; hence, $g_1(\tau)$ is obtained.

There is a complication which may arise in studying porous media. We have implicitly assumed in the derivation of Eq. (31) that the geometry and density of particles of each species is such that there is a statistical sampling of each species in each path, that is, if we double the path length there are twice as many particles of each species con-

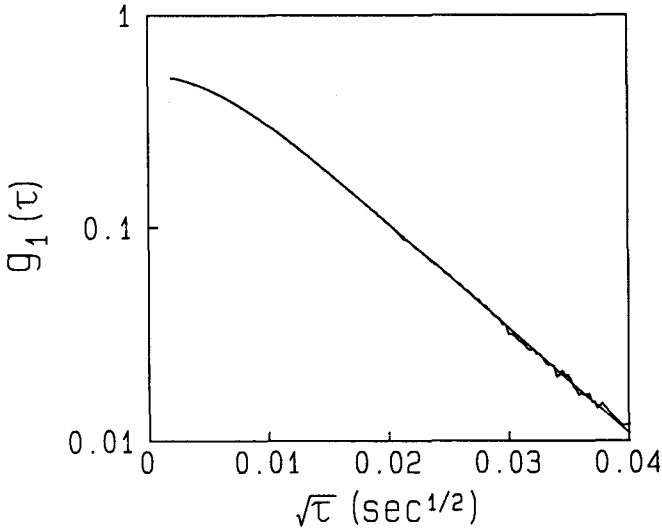

Fig. 16. Heterodyne autocorrelation function *vs* square root time for backscattering from a glass frit with 4–8 μm diameter pores saturated with a $\phi = 0.01$ suspension of 0.497-μm-diameter polystyrene spheres.

tributing to the scattering. If on the other hand we have a very dilute concentration of moving particles in a porous medium, such that all paths sampled by the correlation function involve at most one scattering from a mobile particle, then the description given above is invalid. Instead the correlation function will be like that for the single scattering limit, i.e. like that for QELS. The effect of the scattering from the porous medium will simply be to randomize the direction of incident and scattered wavevectors. Thus the correlation function will have the form of a QELS relaxation averaged over scattering angles and weighted by the form factor for scattering from a single sphere. For spheres much smaller than the wavelength of light, the scattering from a single sphere is isotropic and the average is easily performed:

$$g_1(\tau) = \frac{4\tau_0}{\tau}\left(1 - e^{-\tau/4\tau_0}\right) . \tag{32}$$

For $\tau \ll \tau_0$, $g_1(\tau) \sim \exp(-\tau/2\tau_0)$ and for $\tau \gg \tau_0$, $g_1(\tau) \sim \tau^{-1}$. Figure 17 shows an autocorrelation function obtained from a porous glass

sample with $\sim 5\mu$m-diameter pores which were filled with an aqueous suspension of mobile 0.091μm-diameter polyballs at $\phi = 0.01$. The data were found to be in excellent agreement with Eq. (32) where the value of $\tau_0 = (Dk_0^2)^{-1}$ is given by the free particle diffusion coefficient for the polyballs. This is consistent with the expectation that diffusion should be unimpeded when the pore size is much larger than the mean particle diameter.

6.4. Absorption

In any physical system there will always be absorption of light, either by the scatterers themselves or by the solvent in which they are suspended. Furthermore, the effects of absorption will be enhanced in the multiple scattering limit because the path lengths of the light and the number of scattering events are greatly increased. However, the consequences of absorption for the autocorrelation function can be readily determined within our approach. For any scattering geometry, $P(s)$ is the fraction of the scattered intensity associated with paths of length $s = nl$. With absorption, the intensity of light travelling a path of length s is attenuated exponentially by a factor $\exp(-s/l_a)$, where l_a is the absorption length. Thus, we write $P'(s) = P(s)\exp(-s/l_a)$, where $P(s)$ is determined solely by geometry, as before. Then Eq. (12) has the form:

$$G_1(\tau) = I_0 \int P(s) e^{-s/l_a - (2\tau/\tau_0)s/l^*} ds \ .$$

Since both terms in the exponent are linear in s, the effect of the absorption is mathematically the same as shifting the time scale. Thus all of our previous analysis for different geometries is directly applicable if we simply make the substitution:

$$\tau/\tau_0 \rightarrow l^*/2l_a + \tau/\tau_0 \ .$$

In this case, the form of the autocorrelation function for backscattering becomes

$$g_1(\tau) = \exp\left(-\gamma\sqrt{\frac{6\tau}{\tau_0} + \frac{3l^*}{l_a}}\right) \ . \qquad (33)$$

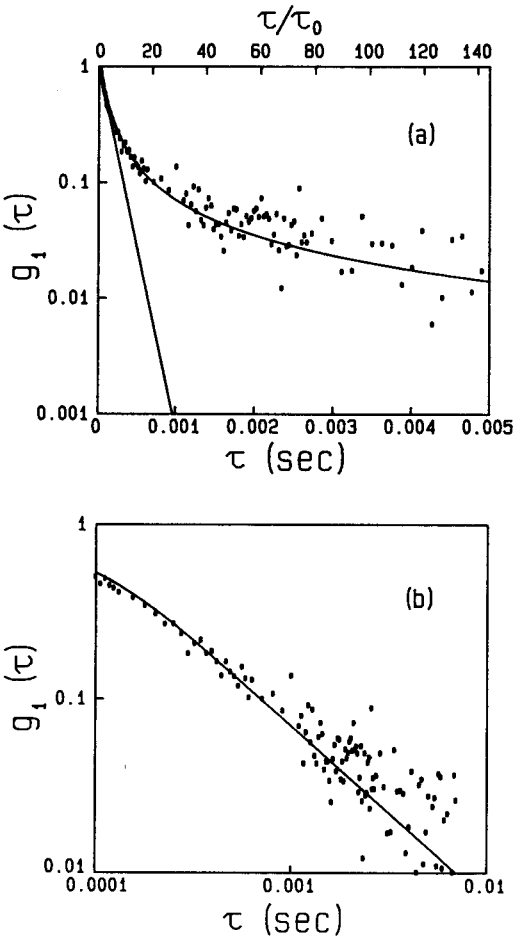

Fig. 17. Heterodyne autocorrelation function *vs* time for scattering from a porous glass sample filled with an aqueous suspension of mobile 0.091-μm-diameter polystyrene spheres at $\phi \simeq 0.01$. Light is multiply scattered by the immobile porous glass but only singly scattered from the mobile polystyrene spheres. (a) Straight line shows first cumulant approximation; (b) τ^{-1} decay at long times.

We illustrate this behavior in Fig. 18, where we show the autocorrelation function obtained in backscattering from 0.497 μm diameter polystyrene spheres with $\phi = 0.01$. The lower curves were obtained upon addition

of varying amounts of methyl red, which absorbs the 488 nm laser light used. The absorption lengths are $l_a = 4.87$ mm for the upper curve and $l_a = 2.53$ mm for the lower curve. Physically, the effect of the absorption is to reduce the contribution of the longer paths to the decay of the autocorrelation function. These paths would otherwise contribute a rapid, initial decay of the correlation function. This effect is clearly evident in Fig. 18 by the rounding of the correlation function at early times.

A comparison of the prediction of Eq. (33) with the data is shown by the solid line in Fig. 18. The theoretical curves do not have any free parameters other than the overall normalization, which is determined by the collection optics, as reflected in $f(A)$. The value of γ used is determined from a measurement without the dye, and the values of l_a for each sample are determined from independent measurements of the transmitted intensity through the sample. The agreement between the theoretical prediction and the data is excellent, confirming the validity of our expression in Eq. (33).

The reduction in the contribution of long paths will also have profound effects in transmission. It will dramatically alter the functional dependence of Γ_1 on L, with Γ_1 becoming linearly dependent on L rather than L^2. This reflects the fact that only the shortest paths can contribute to $G_1(\tau)$ in transmission with absorption, since the longer paths are attenuated. Thus the typical path contribution to the decay will have a length of L rather than $(L/l^*)^2 l^*$.

6.5. Sheared Suspensions

The loss of correlations in the scattered light can be caused by almost any motion of the scattering particles, not just the diffusive motion that we have considered to this point. Convective motion can also cause a loss of correlations. However, uniform motion will not lead to dephasing of multiply scattered light, just as it will not contribute for singly scattered light. For uniform motion, the speckle pattern simply translates with the object. Thus the correlation function will decay only

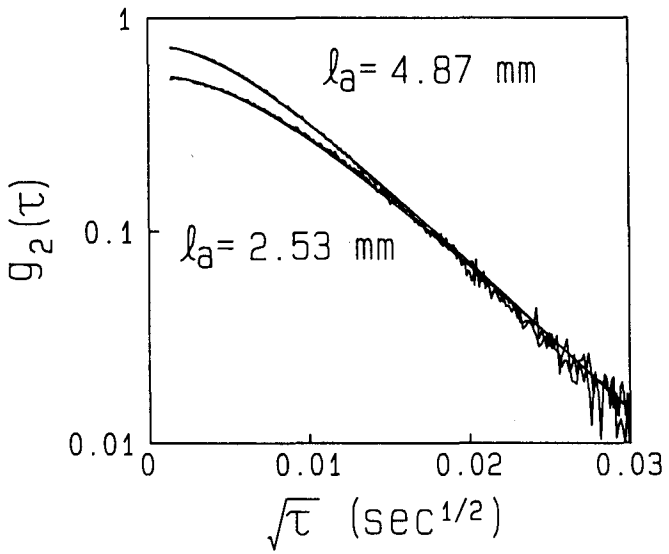

Fig. 18. Intensity autocorrelation functions *vs* square root time for backscattering from samples with absorbing dye in aqueous solution.

as new parts of the sample are introduced into the incident beam or the viewing aperture. By contrast, for relative motion of the particles, the path lengths change and dephasing occurs. The essential difference for convective motion by comparison to diffusive motion is the time dependence of the relative mean square displacement. For convection we have $\langle \Delta r_i^2(\tau) \rangle \propto \tau^2$ whereas for diffusion we have $\langle \Delta r_i^2(\tau) \rangle \propto \tau$. Therefore, we expect the $\sqrt{\tau}$-dependence found up to now to be replaced by a τ-dependence.

The simplest relative motion to treat is that for simple shear such as planar Couette flow.[21] Let us take a velocity profile given by $\mathbf{v} = \Gamma x \hat{\mathbf{e}}_x$, where $\Gamma \equiv \partial v / \partial z$. The relative displacement of a particle consists of a Brownian diffusive term, $\Delta \mathbf{r}_i^B(\tau)$, and a convective shear term, $\Delta \mathbf{r}_i^S(\tau)$. Then, if the Brownian motion is not affected by the laminar shear flow, the total change in phase along a given path of n

scatterers is:

$$\Delta\phi^{(n)}(\tau) = \sum_{i=1}^{n} \Delta\phi_i(\tau) = \sum_{i=1}^{n} \mathbf{q}_i \cdot \Delta\mathbf{r}_i^B(\tau) + \mathbf{q}_i \cdot \Delta\mathbf{r}_i^S(\tau) \ ,$$

where $\mathbf{q}_i = \mathbf{k}_i - \mathbf{k}_{i-1}$. Since the phase is changed only by relative motion of the particles, it is convenient to rewrite the contribution of convection to $\Delta\phi^{(n)}(\tau)$ as

$$\mathbf{q}_i \cdot \Delta\mathbf{r}_i^S(\tau) = \mathbf{k}_i \cdot [\Delta\mathbf{r}_{i+1}^S(\tau) - \Delta\mathbf{r}_i^S(\tau)] = \Gamma\tau k_0 \Lambda_i (\hat{\boldsymbol{\kappa}}_i \cdot \hat{\mathbf{e}}_x)(\hat{\boldsymbol{\kappa}}_i \cdot \hat{\mathbf{e}}_z)$$

where $\Lambda_i \equiv |\Delta\mathbf{r}_{i+1}^S(0) - \Delta\mathbf{r}_i^S(0)|$ is the distance between successive scattering events, $\hat{\boldsymbol{\kappa}}_i$ is a unit vector in the direction of the scattered light, and $\hat{\mathbf{e}}_x$ and $\hat{\mathbf{e}}_z$ are unit vectors in the x and z directions, respectively. This can be rewritten in terms of the polar and azimuthal angles, θ_i and ϕ_i, shown in Fig. 19:

$$\mathbf{q}_i \cdot \Delta\mathbf{r}_i^S(\tau) = \Gamma\tau k_0 \Lambda_i \cos\theta_i \sin\theta_i \cos\phi_i \ .$$

For small particles which scatter light isotropically, the successive $\Delta\phi_i(\tau)$ are uncorrelated and the average of the product in Eq. (3) is once again the product of the average of n independent terms. Since we have assumed that $\Delta\mathbf{r}_i^B(\tau)$ and $\Delta\mathbf{r}_i^S(\tau)$ represent two independent motions, the average over them can be performed independently. We have previously considered the Brownian motion. For the contribution from shear, we perform a moment expansion. Since the leading non-vanishing term in such an expansion is the second moment, we average $\sin^2 2\theta \cos^2\phi$ over the unit sphere and obtain

$$\left\langle \prod_{i=1}^{n} e^{-i\,\mathbf{q}\cdot\mathbf{r}_i(\tau)} \right\rangle = e^{-2[\tau/\tau_0 + (\tau/\tau_s)^2]} \ ,$$

where $\tau_s^{-1} = \Gamma l k_0/\sqrt{30}$ and $l = \langle\Lambda\rangle$ is the scattering mean free path. The total autocorrelation function is once again obtained by summing over all paths with $s = nl$

$$G_1(\tau) = I_0 \int P(s) e^{-2[\tau/\tau_0 + (\tau/\tau_s)^2]s/l} ds \ .$$

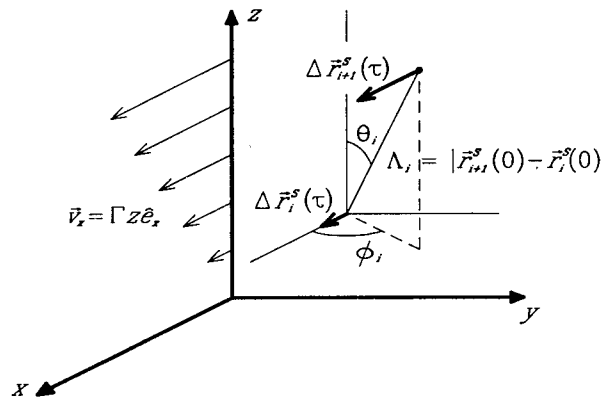

Fig. 19. Scattering geometry for calculation of the autocorrelation functions for shear flow.

For larger particles which scatter light anisotropically, the same results are obtained provided l is replaced by l^* everywhere.[21] Thus, in general

$$\tau_s^{-1} = \Gamma l^* k_0 / \sqrt{30} \; . \tag{34}$$

The form of our results are identical to those previously obtained for diffusion in the absence of shear provided we make the substitution

$$\tau/\tau_0 \rightarrow [\tau/\tau_0 + (\tau/\tau_s)^2] \; . \tag{35}$$

Thus, we can simply adapt our previous results for $G_1(\tau)$ in transmission and backscattering to the case of shear.

In Fig. 20, we show data obtained in backscattering and transmission for a $\phi = 0.02$ suspension of 0.415-μm-diameter polystyrene spheres subject to Poiseuille flow through a 5-cm-long rectangular glass cell. The transverse dimensions of the flow cell were 1mm × 12mm with light incident on the 12-mm face. Velocity gradients were probed along the 1mm dimension in both scattering geometries. The solid curves through the data in Fig. 20 are obtained without any fitting parameters. The shear rate Γ was calculated from measurements of the flow

rate and taken to be the rms average over the 1mm thickness of the cell. The other parameters, γ, l^*, and τ_0, were obtained from measurements without flow. The agreement between theory and experiment is excellent.

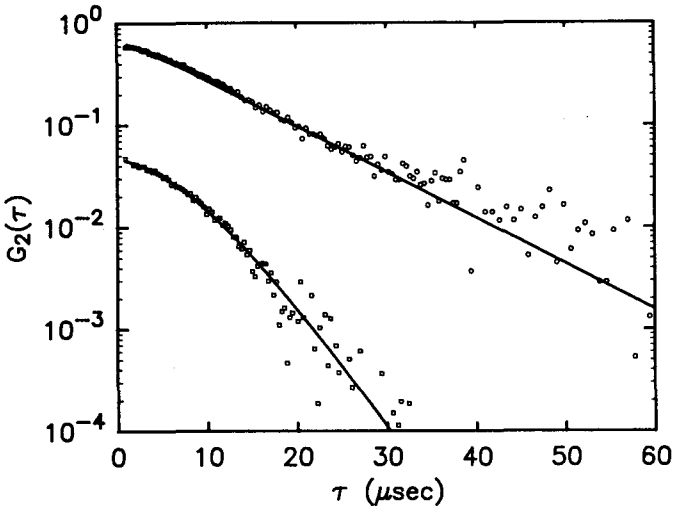

Fig. 20. Intensity autocorrelation functions for backscattering (top) and transmission (bottom) from a $\phi = 0.02$ suspension of 0.415-μm-diameter polystyrene spheres subject to Poiseuille flow.

6.6. Interacting Particles

In the preceding discussion, we have implicitly assumed that the particles which scatter light are completely uncorrelated. Thus, we were able to separately average over the particle positions and the scattering wavevector. However, this is strictly true only in the limit of a dilute, non-interacting suspension of particles. More generally, both the positions and the velocities of the particles are correlated due to their interactions. These effects are particularly important in the dense suspensions for which DWS is ideally suited. The most important interactions are: (a) hard-core repulsion, which is short-range and important at high volume fractions, (b) hydrodynamic interactions, which are long

rate and taken to be the rms average over the 1mm thickness of the cell. The other parameters, γ, l^*, and τ_0, were obtained from measurements without flow. The agreement between theory and experiment is excellent.

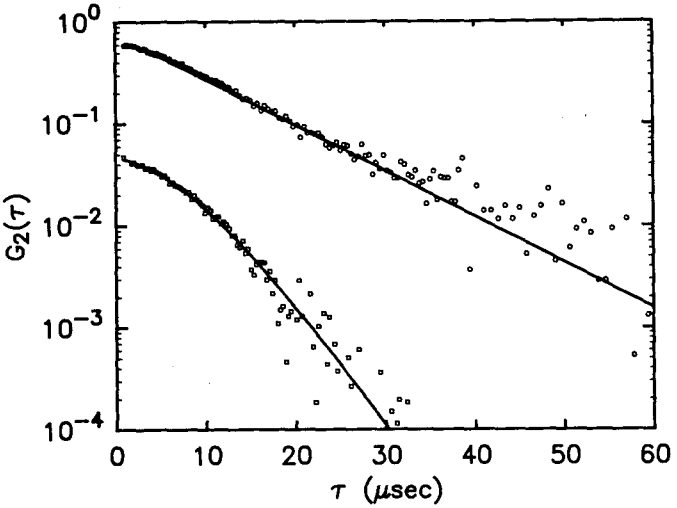

Fig. 20. Intensity autocorrelation functions for backscattering (top) and transmission (bottom) from a $\phi = 0.02$ suspension of 0.415-μm-diameter polystyrene spheres subject to Poiseuille flow.

6.6. Interacting Particles

In the preceding discussion, we have implicitly assumed that the particles which scatter light are completely uncorrelated. Thus, we were able to separately average over the particle positions and the scattering wavevector. However, this is strictly true only in the limit of a dilute, non-interacting suspension of particles. More generally, both the positions and the velocities of the particles are correlated due to their interactions. These effects are particularly important in the dense suspensions for which DWS is ideally suited. The most important interactions are: (a) hard-core repulsion, which is short-range and important at high volume fractions, (b) hydrodynamic interactions, which are long

range but generally become important as the volume fraction increases, and (c) Coulomb repulsion, which can be important even at low volume fractions provided the counterions in solution do not screen the interactions too severely.[22] To fully exploit the potential of DWS, we must consider the consequences of correlations between the particles on the measured autocorrelation functions.

To appreciate the problems of treating interacting systems, it is useful to recall the limiting case of single scattering. Quasielastic light scattering from interacting systems measures the dynamic structure factor, $S(\mathbf{q},\tau)$, defined as,

$$\frac{\langle E(0)E^*(\tau)\rangle}{F(\mathbf{q})} = NS(\mathbf{q},\tau) = \left\langle \sum_{ij=1}^{N} e^{i\,\mathbf{q}\cdot[\mathbf{r}_i(0)-\mathbf{r}_j(\tau)]} \right\rangle ,$$

where the sum is over the N scatterers, $\mathbf{q}$ is the scattering wavevector, $F(q)$ is the form factor of the scatterers and $\langle\,\rangle$ denotes the ensemble average. The dynamic structure factor is related to the Fourier transform of the pair correlation function of scatterers and depends on the interactions.[22] For independent scatterers undergoing Brownian motion, $S(q,0) = 1$ and $S(q,\tau) = \exp(-Dq^2\tau)$; interactions introduce correlations between particle positions and velocities and $S(q,\tau)$ no longer decays exponentially.

For short times, $S(q,\tau)$ can be expressed in terms of $S(q,0)$ and the diffusion coefficient, $D_0 = k_BT/\zeta$, since the particles have moved a distance small compared to the average separation. Here, ζ is the particle friction coefficient corrected for hydrodynamic interactions. Hence, a particle's motion is not yet affected by interaction with its neighbors and the initial decay of $S(q,\tau)$ is determined by the free particle motion.[22] Thus, we have,

$$S(q,\tau) = S(q,0) - q^2\langle r^2(\tau)\rangle/6$$

or, for Brownian motion,

$$S(q,\tau) = S(q,0) - D_s q^2\tau = S(q,0)e^{-D_s q^2\tau/S(q)}$$

which amounts to considering the effects of correlations only on the average positions of the scatterers, and not on their velocities. Thus, the collective diffusion coefficient is

$$D_c(q) = D_s/S(q) \,, \tag{36}$$

where $S(q) = S(q,0)$ is the static structure factor.

Considering now the multiple scattering regime, proper incorporation of the correlations requires that the basic expression for the scattering from particles in the medium be reformulated. Rather than considering the scattering from the individual particles as we have done, we must consider the scattering from the density fluctuations of the correlated particles which are described by $S(q,\tau)$. In general, the range of correlations, ξ, is smaller than the scattering mean free path, so that the multiple scattering is from an ensemble of *independent* cells of size ξ, which are described by the *local* structure factor, $S(q,\tau)$ (Refs. 11,18). One effect of these correlations will be to modify l^* as can be seen directly from its definition, Eq. (9). To include the effects of interactions, we must replace $F(q)$ by the full scattering function, $S(q)F(q)$, giving

$$\frac{l^*}{l} = \frac{2k_0^2\langle S(q)F(q)\rangle}{\langle q^2 S(q)F(q)\rangle} \,. \tag{37}$$

With these modifications, we can adapt our former derivation for the autocorrelation function to the case of interacting particles. The time dependence of the average correlation function for a given path with n cells is

$$\langle \prod_{i=1}^{n} S(q_i,\tau)\rangle / \langle \prod_{i=1}^{n} S(q_i,0)\rangle \,.$$

The normalization insures that this expression goes to 1 as $\tau \to 0$, so that it contains only the time dependence of the autocorrelation function, as modified by the interactions. This allows us to again use the diffusion approximation to determine the intensity of nth order paths,

$$G_1^{(n)}(\tau) = I_0 P(n) \frac{\langle \prod_{i=1}^{n} S(q_i,\tau)\rangle}{\langle \prod_{i=1}^{n} S(q_i,0)\rangle} \,,$$

where $\langle\rangle$ is the average over q weighted by the form factor $F(q)$ and $P(n)$ is the fraction of intensity in nth order paths. Within the diffusion approximation, $P(n) = P(s/l^*) = P(nl/l^*)$, with both l and l^* modified by the static structure factor, $S(q)$. For long paths, the successive q_i are uncorrelated, and the sum over the paths samples all possible q_i, so that we can replace the average of the product by the product of the average,

$$G_1^{(n)}(\tau) = I_0 P(n) \frac{\langle S(q,\tau)\rangle^n}{\langle S(q,0)\rangle^n} .$$

For short times, $\langle S(q,\tau)\rangle / \langle S(q,0)\rangle \simeq 1$, and we express $G_1^{(n)}(\tau)$ as

$$G_1^{(n)}(\tau)\ I_0 P(n) \exp\left[-\frac{nl}{l^*}\frac{l^*}{l}\left(1 - \frac{\langle S(q,\tau)\rangle}{\langle S(q,0)\rangle}\right)\right] ,$$

where we make explicit the fact that nl/l^* is the relevant quantity in the diffusion approximation, since $s = nl$. Comparing this equation to Eq. (8), we find, as shown by MacKintosh and John,[18] it is possible to make the substitution,

$$\frac{2\tau}{\tau_0} \to \frac{l^*}{l}\left(1 - \frac{\langle S(q,\tau)\rangle}{\langle S(q,0)\rangle}\right)$$

in all the expressions for the autocorrelation function $G_1(\tau)$ to correctly account for particle correlations.

Let us now apply this result to the case considered above where $D_c(q) = D_s/S(q)$, or $S(q,\tau) = S(q,0) - D_s q^2 \tau$. Using Eq. (37), we find that the substitution gives[11]

$$\frac{\tau}{\tau_0} \to \frac{\tau}{\tau_0'}$$

with

$$\frac{\tau_0'}{\tau_0} = \frac{\langle q^2 S(q)\rangle}{\langle q^2\rangle} .$$

Thus, interactions do not modify the functional form of $G_1(\tau)$ for short times, and in particular, the square root singularity in backscattering is preserved. Only the time scale of the decay is modified according to the above equation. We can evaluate its modification for

hard core interactions between the scatterers, which are probably dominant for the polystyrene latex suspensions discussed above, where the Coloumb interactions are effectively screened. In this case, the static structure factor is known.[23] For a suspension with $\phi = 0.10$, $S(q)$ increases from 0.45 at $q = 0$ to 1 at $q \sim \pi/R$, where R is the particle radius. We then have to consider the average of $S(q)$, weighted by $q^2 F(q)$. For most of the scatterers we have used, this average emphasizes only the high q region of $S(q)$, where $S(q) \sim 1$, because the diameter is comparable to the wavelength. Thus, the effect of the spatial correlations, which are reflected by the behavior at low q, will tend to be averaged out. Then we expect the time scale of the decay to be only slightly modified with respect to the non-interacting case. This probably explains why the data of Fig. 10, although obtained with suspensions of $\phi = 0.1$, fall on the same curve when the time scale is scaled by the free particle diffusion time, τ_0.

By contrast, the long time behavior of $G_1(\tau)$ can be dramatically affected by the interactions. To illustrate this, we consider the autocorrelation functions obtained from a colloidal crystal. This is achieved by reducing the concentration of counterions in a suspension of polystyrene latex to the point where the Coulombic repulsion between the particles is sufficiently long range that the balls crystallize. In Fig. 21, we contrast the autocorrelation functions measured in backscattering from a non-interacting colloidal suspension and a colloidal crystal. We again use a logarithmic plot of $g_2(\tau)$ as a function of the square root of delay time. Both samples were comprised of 0.215 μm diameter polystyrene spheres at the same volume fraction, $\phi = 0.10$. The only difference between the samples is the range of the screened Coulomb interactions, which is experimentally controlled by the concentration of counterions which have been reduced in one sample, causing it to crystallize. However, the autocorrelation functions are markedly different. The autocorrelation function of the colloidal liquid decreases exponentially with the square root of delay time, as expected. By contrast, $g_2(\tau)$ for the colloidal crystal exhibits an initial rapid decay at the very early times,

but then saturates, and does not decay to the baseline even at long time scales. To ensure that a correct measure of the baseline is obtained for these samples, data were taken at several different positions on the sample and the separate results were averaged.[24]

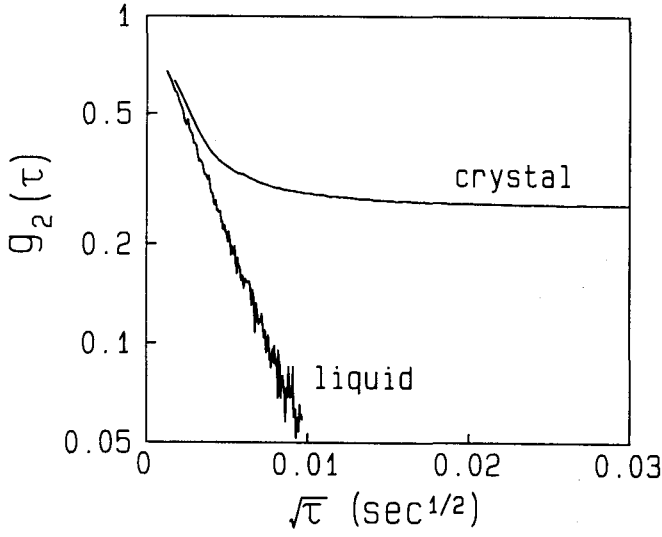

Fig. 21. Intensity autocorrelation functions from a weakly-interacting colloid (liquid) and from a strongly interacting colloid (crystal). Both suspensions consist of 0.215-μm-diameter spheres with $\phi = 0.10$.

This behavior is consistent with our expectations for the average displacement of the particles in a colloidal crystal. At early times they will move relatively freely, with the same diffusion coefficient as for the non-interacting particles. However, as their mean displacement approaches some fraction of the interparticle separation, they will feel the Coulombic repulsion of their neighbors and will be unable to move further. This is reflected in a decrease in their diffusion coefficient as time increases. The backscattering autocorrelation function reflects this directly. It probes a wide range of path lengths, and consequently a wide range of decay times. At early times, the very rapid decay reflects the contribution of the long paths, which consist of many scattering events,

so that each ball need move only a small amount. This occurs very rapidly, since the particles are diffusing relatively quickly. By contrast, at later times, the slow decay reflects the contribution of the very short paths, which consist of a small number of scattering events, so that each ball must move a greater distance to cause the decay. This occurs on a much longer time scale due to the repulsive interactions.

These results illustrate the potential power of DWS in studying systems with interactions between the particles. There are clearly many other very interesting interacting systems that can be studied by means of DWS. However, caution must be exercised in the interpretation of the results in determining the exact consequences of the correlations of both the positions and motions of the particles. Indeed, considerable work remains to be done to fully determine the extent to which the relatively simple interpretations used here are valid.

7. CONCLUSIONS

In this chapter, we have presented a discussion of the temporal correlations of multiply scattered light. A phenomenological derivation of the autocorrelation functions of the scattered intensity is used to obtain expressions for several experimentally important geometries. This derivation specifically exploits the diffusion approximation for the transport of light in a multiple scattering medium. The geometries considered are transmission through a slab and backscattering from a slab. The expressions obtained are compared to experimental data and excellent agreement is found.

The temporal autocorrelation functions directly reflect the motion of the scatterers in the medium. By using our expressions, we are able to relate the temporal fluctuations to this motion and thereby obtain useful information about the dynamics of the scattering medium. This provides a new method for studying the dynamics of dense suspensions, which we have called Diffusing Wave Spectroscopy. We have demonstrated the utility of DWS by applying it to measure the particle size in concentrated suspensions, as well as to study the dynamics of par-

ticles in porous media and under shear. We have also considered the consequences of particle interactions, and the resulting correlations in the particle positions and velocities, on the measured autocorrelation functions.

Finally, we have shown that the temporal autocorrelation functions probe the same combination of diffusing light paths as does the enhancement of the static backscattering. This allows us to draw an elegant analogy between these measurements, and thereby use the measured autocorrelation functions as a sensitive probe of the physics of the multiple scattering of light.

ACKNOWLEDGEMENTS

We have benefited greatly from valuable discussions with many of our colleagues. In particular, we wish to thank Michael Stephen who performed many of the important first calculations of the autocorrelation functions, and Fred MacKintosh and Sajeev John who were instrumental in determining the correct form of the autocorrelation function in backscattering. The measurements for the particles in a porous medium were obtained in collaboration with Penger Tong and Walter Goldberg; those for particles under shear with Xiao-Lun Wu; those for interacting particles with Xia Qiu and Dan Ou-Yang; and those for the dependence of γ on l^*/l with Jixiang Zhu. We also acknowledge many fruitful discussions with Fred MacKintosh and Rudolf Klein.

REFERENCES

1. B. J. Berne and R. Pecora, *Dynamic Light Scattering: With Applications to Chemistry, Biology, and Physics* (Wiley, New York, 1976).
2. N. A. Clark, J. H. Lunacek and G. B. Benedek, *Am. J. Phys.* **38** (1970) 575.
3. J. K. G. Dhont, in *Photon Correlation Techniques in Fluid Mechanics*, edited by E. O. Schulz-DuBois, (Springer-Verlag, Berlin, 1983).
4. G. Maret and P. E. Wolf, *Z. Phys.* **B65** (1987) 409.
5. M. Rosenbluh, M. Hoshen, I. Freund and M. Kaveh, *Phys. Rev. Lett.* **58** (1987) 2754.

6. M. J. Stephen, *Phys. Rev.* **B37** (1988) 1.
7. D. J. Pine, D. A. Weitz, P. M. Chaikin and E. Herbolzheimer, *Phys. Rev. Lett.* **60** (1988) 1134.
8. D. J. Pine, D. A. Weitz, P. M. Chaikin and E. Herbolzheimer, in *Proceedings of the Topical Meeting on Photon Correlation Techniques and Applications*, edited by A. Smart and J. Abbiss. (Optical Society of America, Washington, 1988).
9. M. P. van Albada and A. Legendijk, *Phys. Rev. Lett.* **55** (1985) 2692.
10. P. E. Wolf and G. Maret, *Phys. Rev. Lett.* **55** (1985) 2696.
11. G. Maret and P. E. Wolf, (*to be published*).
12. A. A. Golubentsev, *Zh. Eksp. Theor. Fiz.* **86** (1984) 47 [*Sov. Phys. JETP* **59** (1984) 26].
13. D. Pine and E. Herbolzheimer, *private communication.*
14. Short paths can only occur in a backscattering geometry. In this case the distribution of $\mathbf{q}_i$ can have a significant contribution from single scattering through 180°, $q \sim 2k_0$.
15. A. Ishimaru, *Wave Propagation and Scattering in Random Media, Vol. I* (Academic, New York, 1978).
16. P. E. Wolf, G. Maret, E. Akkermans and R. Maynard, *J. Phys.* (France) **49** (1988) 63.
17. L. Landau and E. M. Lifshitz, *Statistical Physics* (Pergamon, Oxford, 1980), p. 396.
18. F. MacKintosh and S. John, *Phys. Rev.* **B40** 2383 (1989).
19. S. Milner, *private communication.*
20. See, for example, articles by N. Ostrowsky and D. Sornette or M. Bertero and E. R. Pike in *Photon Correlation Techniques in Fluid Mechanics*, edited by E. O. Schulz-DuBois (Springer-Verlag, Berlin, 1983).
21. X. L. Wu, D. J. Pine, P. M. Chaikin, J. S. Huang and D. A. Weitz, *J. Opt. Soc. Am. B* in press.
22. P. N. Pusey and R. J. A. Tough, in *Dynamic Light Scattering*, edited by R. Pecora (Plenum, New York, 1985) p. 85.
23. M. S. Wertheim, *Phys. Rev. Lett.* **10** (1965) 321.
24. P. N. Pusey and W. van Megan, *Phys. Rev. Lett.* **59** (1983) 2083.